TU Delft

Delft University of Technology

An artificial potential field approach for virtual coupling train control with complete braking curve supervision

Ji, Yuqing; Quaglietta, Egidio; Goverde, Rob M.P.; Ou, Dongxiu

DOI
10.1016/j.trc.2025.105050

Publication date
2025

Document Version
Final published version

Published in
Transportation Research Part C: Emerging Technologies

Citation (APA)
Ji, Y., Quaglietta, E., Goverde, R. M. P., & Ou, D. (2025). An artificial potential field approach for virtual coupling train control with complete braking curve supervision. *Transportation Research Part C: Emerging Technologies*, *173*, Article 105050. https://doi.org/10.1016/j.trc.2025.105050

Important note
To cite this publication, please use the final published version (if applicable).
Please check the document version above.

Copyright
Other than for strictly personal use, it is not permitted to download, forward or distribute the text or part of it, without the consent of the author(s) and/or copyright holder(s), unless the work is under an open content license such as Creative Commons.

Takedown policy
Please contact us and provide details if you believe this document breaches copyrights.
We will remove access to the work immediately and investigate your claim.

This work is downloaded from Delft University of Technology.
For technical reasons the number of authors shown on this cover page is limited to a maximum of 10.

Green Open Access added to TU Delft Institutional Repository

'You share, we take care!' - Taverne project

https://www.openaccess.nl/en/you-share-we-take-care

Otherwise as indicated in the copyright section: the publisher is the copyright holder of this work and the author uses the Dutch legislation to make this work public.

Transportation Research Part C 173 (2025) 105050

Contents lists available at ScienceDirect

Transportation Research Part C

journal homepage: www.elsevier.com/locate/trc

An artificial potential field approach for virtual coupling train control with complete braking curve supervision

Yuqing Ji [a,b,*], Egidio Quaglietta [b], Rob M.P. Goverde [b], Dongxiu Ou [a]

[a] Shanghai Key Laboratory of Rail Infrastructure Durability and System Safety, College of Transportation Engineering, Tongji University, Shanghai, China

[b] Department of Transport and Planning, Delft University of Technology, Delft, the Netherlands

ARTICLE INFO

Keywords:
Virtual coupling
Dynamic safety margin
Complete braking curve supervision
Train control
Artificial potential field

ABSTRACT

In response to the escalating demand for rail transport, the concept of Virtual Coupling (VC) train operations is progressively gaining ground within the railway sector. The concept of VC aims at reducing safe train separation to less than the absolute braking distance by letting trains move synchronously in radio-connected convoys. One of the major concerns associated with VC is ensuring safe train separation considering realistic risk factors, such as heterogeneous train braking performances and varying track conditions. To address such a safe train separation problem under VC, this paper proposes a novel train control model based on the Artificial Potential Field (APF) method to safely supervise the complete braking process of trains moving in a VC convoy. The proposed model uses a homogeneous strip representation of train length and a Dynamic Safety Margin (DSM) to take into account accurate train dynamics as well as potential risk factors, due to different train acceleration/braking rates, communication delays, unexpected emergency train braking applications, and position measurement errors. The method has been applied to the case of a high-speed line in China. Results show that the APF-based control method can effectively adapt to real-time variations in train dynamics and the operational environment to safely supervise the complete train braking process and avoid collisions even in the case of unplanned emergency braking applications. The proposed APF-based approach shows promising real-time performance which can further contribute to advancing the state of the art on safe train control under VC signalling.

1. Introduction

The increase in the rail transport demand poses a challenge for infrastructure managers to increase the capacity of existing railway networks while keeping or even improving train service performance. To address this challenge, the railway industry is exploring next-generation signalling systems like Moving Block (MB) (Basile et al., 2022) and Virtual Coupling (VC) (Aoun et al., 2023), which migrate vital track-side equipment to the onboard of trains to reduce safe train separation. In MB, the safe train separation is reduced to an absolute braking distance plus a safety margin by exploiting a Vehicle-to-Infrastructure (V2I) radio communication layer as well as onboard devices responsible for monitoring train integrity and supervising speed. The concept of VC builds upon the MB framework by incorporating Vehicle-to-Vehicle (V2V) communication. This extension opens up the possibility of further reducing the safe train

* Corresponding author.
E-mail address: jiyuqing@tongji.edu.cn (Y. Ji).

https://doi.org/10.1016/j.trc.2025.105050
Received 13 March 2024; Received in revised form 24 November 2024; Accepted 15 February 2025
Available online 25 February 2025
0968-090X/© 2025 Elsevier Ltd. All rights are reserved, including those for text and data mining, AI training, and similar technologies.

separation down to a relative braking distance (RBD), which is the difference of the braking distances of successive trains plus a safety margin to the rear of the leading train (Ning, 1998, Bock, 1999). Moreover, V2V communication allows forming convoys where trains can move synchronously (Quaglietta et al., 2022).

International research programmes such as Shift2Rail (2018) and Europe's Rail (2018) have been investigating the impact that VC signalling could have on the rail transport sector. Some preliminary research (Quaglietta et al., 2020, Quaglietta et al., 2022) has investigated principles for safe train operations under VC as well as the capacity benefits that such a concept could bring versus both conventional fixed-block and moving-block signalling. A relevant stream of research (Ketphat et al., 2022, Liu et al., 2023) on VC operations aimed at developing train control algorithms which can effectively supervise safe train separation while regulating coupling/decoupling transitions of trains moving in VC convoys. In a VC train convoy where trains are expected to follow each other at a significantly shorter distance compared to those in MB, the risk of collisions significantly increases if the train control fails to respond promptly to changes in the safe train separation requirement due to e.g., changes in train dynamics, varying track conditions, rolling stock heterogeneity of trains in the VC convoy. Therefore, the main challenge of train control under VC is the need to provide safe control indications to trains compatibly with the real-time nature of coupling/decoupling procedures and the short train separations while considering realistic operational and risk factors.

In general, most existing train control methods proposed for VC include modelling assumptions, approximations or simplifications about train dynamics or the operational environment (e.g. latency of the communication layer, control delays, track characteristics) which might limit their applicability in a real-life setup. First, current methods (Cao et al., 2022, Cao et al., 2021, Chen et al., 2020, Felez et al., 2019) often involve a mass-point representation of trains which cannot capture realistic overall motion resistances of trains, especially on tracks with irregular gradient profiles. This would be more accurately described by a homogeneous strip model (Fan, 2012) representing each train as a set of connected segments divided by knickpoints of slopes or curves. Addressing those modelling issues is significant for an accurate evaluation of the capacity advantages and technical challenges that VC will introduce.

Second, existing literature (Felez et al., 2019, Di Meo et al., 2019, Zhang et al., 2023, Ning et al., 2023) mainly refers to homogeneous VC train convoys (i.e. trains having similar rolling stock characteristics). Although using homogenous trains simplifies the train separation problem for both the separation calculation and control, industrial development of VC can only occur if the concept proves to be applicable in multiple rail market segments including main-line and regional lines which mostly feature heterogeneous trains. Some promising research (Su et al., 2023, Xun et al., 2020, Luo et al., 2023) is available on safe train control in heterogeneous convoys considering different service/emergency braking capabilities which are mostly constant values. However, the train heterogeneity can be more realistically represented if varying braking capabilities of trains are modelled by considering the actual braking rate function which depends on the train speed.

Third, some research (Wu et al., 2023, Liu et al., 2023, Ketphat et al., 2022, Park et al., 2020, Quaglietta et al., 2020) has developed different methods to define train separation under VC either by exploiting constant or dynamic train separation. Since different train speeds and positions can lead to varying safety margins, a static safety margin may not be able to guarantee a safe train separation in the presence of any of those risk factors. However, literature on the use of the Dynamic Safety Margin (DSM) (Quaglietta et al., 2022) which is a time-varying safety margin taking into account realistic operational risk factors is still limited and would need to be further investigated for a safe deployment of VC operations. So far, most existing VC train control algorithms do not indeed consider a DSM to safely separate trains in the presence of a comprehensive series of risk factors due to extended train reaction times, V2V communication latencies, sudden emergency train braking, heterogeneous train characteristics, speed and position measurement errors. While some of these factors have been partially addressed in the literature, most studies only consider part of them, e.g., Felez et al. (2019) consider only the train positioning error. Instead, this paper addresses all of these risk factors and additionally, newly introduces varying track conditions (e.g., gradient changes) into the DSM to account for a more realistic VC train operational environment.

An additional shortcoming of most existing VC train control algorithms is that they aim at ensuring safe train separation only considering the position that trains will have at the end of the braking process (called End Braking Point Supervision (EBPS) hereafter) (Liu et al., 2023, Felez et al., 2019, Quaglietta et al., 2020, Park et al., 2020, Quaglietta et al., 2022, Cao et al., 2021), which does not necessarily exclude that trains might instead collide during the braking process itself, due to e.g. varying braking performances and unfavourable track resistances (e.g. steep downhills). In such a context it is essential that the train control is able to supervise the safe train separation across the complete braking process while taking into account transient track and rolling stock conditions as well as realistic risk factors including failure events to signalling and communication components. A safe implementation of VC train control algorithms shall hence refer to a Complete Braking Curve Supervision (CBCS) which ensures safe train separation from the start until the end of the braking processes of the trains in a VC convoy. However, only a few approaches that have been proposed in the literature refer to CBCS, such as works by Chai et al. (2023) and Wang et al. (2022), however, these studies mainly assume flat tracks and do not account for train resistances due to varying track layouts, e.g. gradients and curves.

The research in this paper addresses the above-reported limitations by proposing an innovative VC train control algorithm for safely supervising the complete braking process of trains while considering: i) realistic dynamics of physically-coupled cars in a train over varying track alignments, ii) realistic VC convoy heterogeneity under transient train speeds, iii) risk factors due to sudden emergency braking, latencies in train control and communication, position/speed measurement errors and unfavourable track conditions.

A CBCS train control algorithm is hence developed which uses a homogeneous strip train model with detailed braking characteristics while including a dynamic safety margin to dynamically adapt safe train separation in case of risk factors such as unforeseen emergency braking, heterogeneous train braking performances, and malfunctions/faults in the signalling and communication systems. The CBCS with dynamic safety margin is performed by introducing a novel approach based on Artificial Potential Field (APF) which has proven in other research fields to be particularly efficient for real-time applications where the short response time of the controller is essential, such as in VC operations. The proposed method has been applied to a real case of a high-speed rail network in China. An

extensive comparative analysis is provided illustrating the impacts on safe train separation when using an end braking point supervision versus a complete braking curve supervision.

The main contributions of this research to the state of the art can hence be summarised as follows:

i) An artificial potential field-based approach with dynamic impact distance is introduced which allows efficient train control in line with the real-time application requirements of virtual coupling while effectively supervising safe train separations without triggering emergency braking actions;
ii) A complete braking curve supervision-based dynamic safe train separation calculation method is proposed which takes into account real-line conditions, risk factors, heterogeneous train characteristics as well as realistic speed-dependent train braking capabilities;
iii) A homogeneous strip train model is used for the first time to consider the combined effect of train length and varying track alignments when controlling train separation in a VC convoy.

The remainder of this paper is organized as follows: Section 2 offers a comprehensive literature review. Section 3 introduces the proposed methods and models. Section 4 contains simulations and their respective results. Finally, Section 5 provides the conclusions of this paper and future research directions.

2. Literature review

2.1. Train separation principles

The development of railway signalling systems has seen a significant transformation over the years, progressing from Fixed Block (FB) signalling to Virtual Block (VB), Moving Block (MB), and recently to Virtual Coupling (VC). These transitions represent substantial advancements in railway safety, capacity, and efficiency.

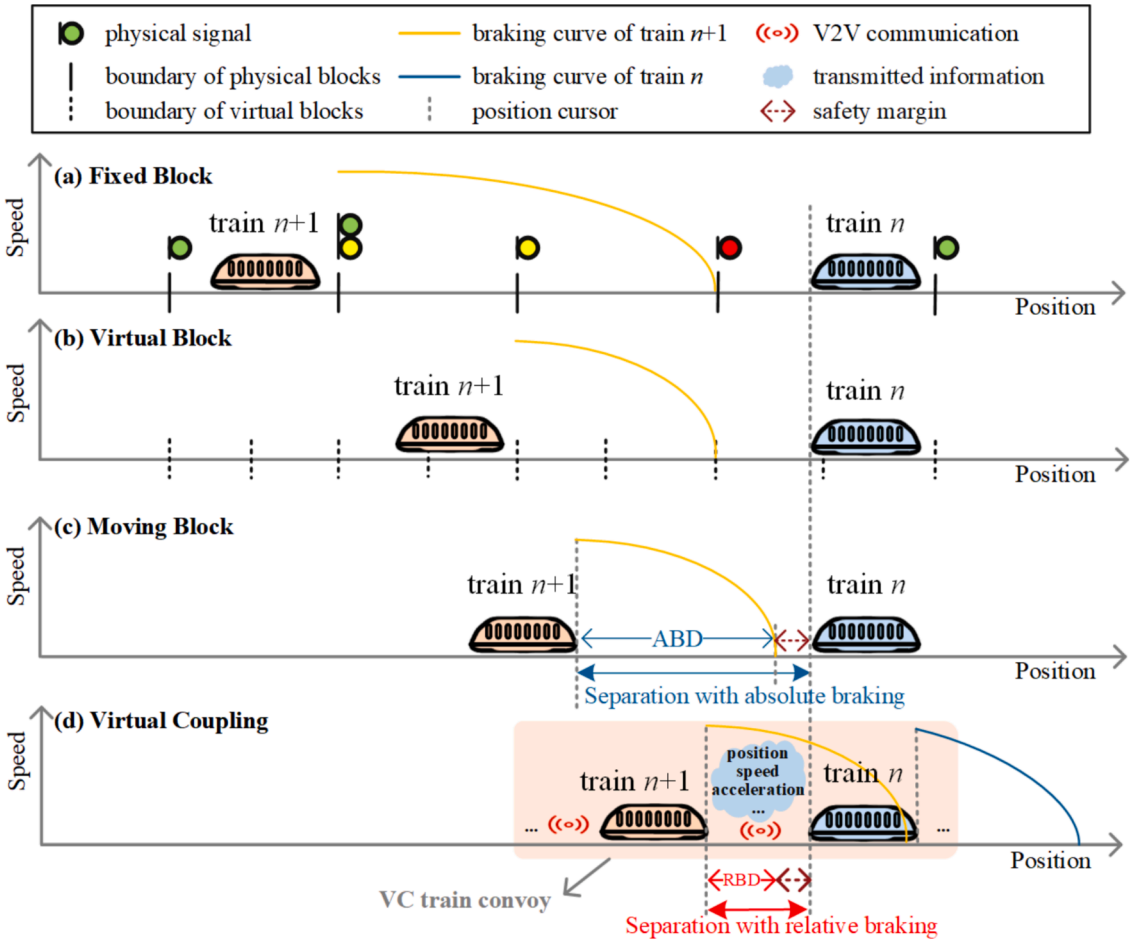

Fig. 1. Comparison of different train separation principles.

In conventional FB multi-aspect signalling (Fig. 1(a)), train separation distance is primarily determined by the number of signal aspects. For instance, in a four-aspect FB system, there are four kinds of signal aspects including: (1) Stop (red), indicating stop before the signal; (2) Approach (yellow), indicating that the train is approaching a red signal and the train needs to reduce speed and prepare to stop before the red signal; (3) Advance approach (double yellow, or yellow and green) (e.g. in Chinese Train Control System (CTCS) Level 0/1/2), preannouncing the approach signal and that the train must stop in two blocks. Therefore, trains should reduce speed, if needed, to reach a target speed at the approach signal from which the train can brake to a standstill in front of the 'stop' signal; (4) Proceed (green), indicating 'clear,' with no need to apply brakes (de Rivera and Dick, 2021). In this four-aspect fixed-block system, the train separation should contain at least two blocks without reducing regular operational train speeds (for sufficient low operational speeds, the train separation may be reduced to at least one block).

To reduce train separation, the rail industry has actively investigated more advanced train signalling systems. For instance, VB signalling, as shown in Fig. 1(b), divides the rail track into logical blocks of specific lengths that allow significantly shorter blocks than conventional FB systems. VB is an intermediary step that introduced the concept of monitoring train-rear positions through onboard equipment and sensors rather than trackside train detection (Chen et al., 2019). This allows for more precise control of train movements and improved capacity.

As the lengths of virtual blocks are further reduced (e.g. approaching zero), the train separation achievable under VB becomes increasingly comparable to that of the MB system. This makes the VB resemble MB signalling (Dick et al., 2019) (see Fig. 1(c)), where the separation between two consecutive trains can reach the Absolute Braking Distance (ABD) which is defined as the braking distance of the following train, plus a margin attached to the rear of the preceding train out of safety concern. MB signalling marks a significant advancement in train separation reduction and it has gained widespread acceptance and popularity in urban railways (Versluis et al., 2024).

Essentially, FB, VB, and MB share the concept of absolute braking. However, Virtual Coupling (Flammini et al., 2018), as shown in Fig. 1(d), allows reducing the train separation to a far shorter one than an absolute braking distance by using relative braking distance, which is an innovative next-generation signalling concept that exploits Vehicle-to-Vehicle (V2V) communication to combine trains in a virtually-coupled train set.

2.2. Train separation under virtual coupling

Most literature adopts End Braking Point Supervision (EBPS)-based approximate train separation for trains under VC considering only flat tracks and without (or with limited) risk factors. Wu et al. (2023) set the desired train headway under VC as a space constant according to $10 \sim 15$ % variations for the emergency braking distance. Liu et al. (2023) define the desired gap for two adjacent trains under VC as the difference between the emergency braking distances of the following train (called follower hereafter) and the leading train (called leader hereafter) plus a safety margin concerning system and communication delays and measurement errors of speed or position depending only on the follower's kinematics. Similarly, this kind of definition can also be found in works by Chen et al. (2020) and Su et al. (2022). Based on Ning's definition of the relative braking distance (Ning, 1998), Ketphat et al. (2022) modified the minimum separation for trains under VC, in which the acceleration and braking rates of all trains in the same convoy are assumed to be the same, and the actual operational line condition is not discussed when calculating the minimum safe distance. Park et al. (2020) also proposed a gap reference generation method for different specific states including merging, platooning, and decoupling, taking into account uncertainties of emergency braking deceleration, and errors of positioning and velocity measurement. In the work by Quaglietta et al. (2020), a multi-state train-following model was developed for VC, considering a constant safety margin. This model was extended with a dynamic safety margin (DSM) (Quaglietta et al., 2022) which varies over time based on real-time train kinematics of both the leader and the follower to account for real-life risk factors such as communication update delays, train positioning errors, train control delays and sudden emergency train braking applications.

Another promising stream of related research on DSM under VC is instead considering the Complete Braking Curve Supervision (CBCS) which ensures the safe train separation throughout the entire braking process. Wang et al. (2022) proposed a space–time interval-based calculation method of the minimum safe distance between trains under VC to avoid train collisions during the calculated emergency braking process of both the leader and the follower. This model is further illustrated in the work by Chai et al. (2023) where a relative operation-based separation (ROS) model is proposed to compute the safe separation between VC trains assuming an emergency brake in the follower and the worst-case operation of the leader. The DSM model in Quaglietta et al. (2022) does not rely on EBPS but instead, the model analyzes and calculates each risk factor-concerned safety margin separately. However, in these papers, the varying track conditions including irregular gradient and curvature profiles during the whole assumed service/emergency/worst-case braking processes of trains are not included in the calculation.

Generally, in most studies (Liu et al., 2023, Felez et al., 2019, Quaglietta et al., 2020, Park et al., 2020, Cao et al., 2021), the minimum safe train separation $d_{\min}$ under VC (with the speed of the follower at v^{fol} and the speed of the leader at v^{lead}) is determined by using EBPS which can be represented as $d_{\min}\left(v^{\text{fol}}, v^{\text{lead}}\right) = sm + \max\left(S^{\text{fol}}_{\text{brake}}\left(v^{fol}\right) - S^{\text{lead}}_{\text{brake}}\left(v^{\text{lead}}\right), 0\right)$, where sm is the safety margin concerning some risk factors; $S^{\text{lead}}_{\text{brake}}\left(v^{\text{lead}}\right)$ is the total emergency braking distance of the leader assuming the leader implements an emergency braking rate at speed v^{lead}; $S^{\text{fol}}_{\text{brake}}$ is the total emergency braking distance (or the total service braking distance) assuming the follower implements an emergency braking rate (or a service braking rate) at speed v^{fol}. Among these studies, based on this EBPS method for train separation under VC, some studies (Park et al., 2020, Cao et al., 2021) take into account tracks with gradients or curves and some risk factors such as sudden emergency braking or communication delay.

However, EBPS-based train control poses safety concerns as it only supervises safe train separation at the end of the braking process and disregards train heterogeneities, transient track conditions (e.g. unfavourable slope profile) or events (e.g. prolonged train reaction times or temporary reduction of braking capabilities), which may instead lead trains to collide during the braking itself. A Complete Braking Curve Supervision is instead essential for a signalling system like VC where train separations become shorter than an absolute braking distance. Therefore, the model proposed in this research refers to the supervision of the complete braking curves of trains under VC while including the dynamic safety margin defined in Quaglietta et al. (2022) to account for risk factors which may occur in real VC rail operations.

2.3. Algorithms for safe train control under virtual coupling

In a virtually coupled train convoy, where trains are following each other up to a relative braking distance, the risk of train collision rises if the train control model does not take realistic train operation conditions into account (e.g. the real line resistance), or the potential risk factors such as the leader coming to a sudden triggering of an emergency braking action, especially when trains with heterogeneous braking performances follow each other in a virtually coupled convoy. Therefore, safe train control is crucial for trains under VC to prevent running collisions within train convoys and avoid catastrophic consequences caused by the impact.

Prediction-based control methods such as Model Predictive Control (MPC) have been successfully used in many industrial applications. This is a control algorithm that relies on the iterative solution of an optimization problem based on the predicted states over a receding horizon according to the system model to compute a control input at each sampling point. For train control under VC, some research (Chen et al., 2020, Felez et al., 2019) aimed to solve train collision problems using the MPC method. Chen et al. (2020) proposed a multi-train collision protection control method based on MPC for Virtual Coupling. This method considers minimizing the total relative kinetic energy of a virtually coupled train formation as the optimal control target to ensure the safety of trains. Felez et al. (2019) extended the MPC into a decentralized framework for each train in a convoy under VC, which guarantees non-collision full stop of a follower even if the leader implements emergency braking, however, with a computation time of obtaining the optimal control reaching 709 s covering a distance of 3.7 km. Though MPC offers superior optimal control performance and is adept at managing nonlinear systems and constraints, it is burdened by high computational complexity when increasing train numbers or the prediction horizon (Felez et al., 2019), and increased computation time in nonlinear systems (Ferreau et al., 2008), in which the performance of MPC can be significantly influenced by initial conditions whose changes from one optimization problem to the next one are usually unpredictable (Diehl et al., 2009) which can further result in uncertain computation times at each step. These factors can introduce potential risks to the safe control of trains separated by very short spacing under VC, which demands a high level of real-time control capability.

Non-predictive control methods such as Sliding Mode Control (SMC) provide better real-time control performance than prediction-based control methods. Liu et al. (2023) and Park et al. (2020) proposed a robust gap controller that is based on SMC to apply to a follower to maintain virtually coupled states with a desired separation distance considering uncertainties including time-varying measurement delay and line disturbances. SMC requires very low calculation complexity (Rubagotti et al., 2010) and exhibits the advantage of high convergence speed in nonlinear control problems (Liu et al., 2023). However, the imperfection of SMC arises when the state trajectory reaches the sliding mode surface and then tends to approach the equilibrium point by oscillating back and forth on both sides, resulting in chattering or small fluctuation.

The Artificial Potential Field (APF) (Khatib, 1986) method is also a non-predictive control approach that exhibits robustness in handling control and sensing errors, making it well-suited for adapting to changing targets and dynamic obstacles. Cao et al. (2021) proposed a Generalized Predictive Control (GPC) model and used mixed APF to perform cooperative control and prevent collisions of trains under VC. According to the simulation results, the minimum train separation distance can be controlled within one meter when the train pulls in and stops, which seems to be a promising result. Cao et al. (2022) further developed and improved the APF model by using a time-varying parameter potential field function to realize anti-collision control of trains under VC. However, the constructed repulsive APF functions in their papers refer to an EBPS-based train separation without taking into account a DSM to address comprehensive risk factors and track conditions during the whole assumed braking process of trains. Moreover, their APF model is based on a tailored application which uses a hyperbolic tangent (tanh) function and also, it involves a set of other additional parameters which are not found suitable to our model and not immediate to evaluate/calibrate. An improved APF control method for train collision avoidance under VC is also proposed by Guo and Li (2023), where the safe coupling/decoupling processes are guaranteed for permanent magnetic maglev trains under VC. However, the repulsive radius, which is the distance from the repulsive point to where the repulsive force becomes negligible (referred to as the impact distance hereafter), remains constant. This, however, may not be applicable under VC since the DSM between trains varies during practical operation particularly when there are changes in e.g. train speed or track gradient. Other safe control algorithms for trains under VC such as mixed control methods and machine learning-based control methods (Wang et al., 2020, Su et al., 2022) are emerging.

This paper proposes an APF-based train controller under VC, incorporating a dynamic impact distance to the APF based on the Gaussian function which is proved in the field of road transport (Wolf and Burdick, 2008) to be effective in vehicle control under traffic conditions that are similar to those for VC in the railway field. The proposed method takes into account a wide range of real-life track conditions and risk factors as well as train heterogeneities. Furthermore, the DSM for trains in the proposed controller under VC respects a CBCS-based method. This approach not only facilitates effective safe control and collision avoidance for heterogeneous train operations on real tracks in the presence of realistic factors but also reduces computation time when compared to traditional prediction-based optimal control methods.

2.4. Algorithms for multi-agent system control

Virtual Coupling, where V2V communication is used to create a radio-linked VC convoy, shares similarities with the concept of a Multi-Agent System (MAS). A MAS is a computational system composed of multiple intelligent agents or entities that interact with each other in a networked environment. These agents can be software entities, robots, or even humans (Xue et al., 2010). In the context of this paper, the agents represent trains under VC within the convoy.

In MAS, Virtual Structures (VS), Graph Theory (GT), Reinforcement Learning (RL), and APF methods are common solutions to formation control problems, see Table 1:

(a) For the virtual structures method, the core concept revolves around designating a virtual leader (Porfiri et al., 2007) or a virtual coordinate frame (Ren, 2008) to serve as a central reference point for the entire group, allowing each vehicle to establish its desired states concerning this virtual structure. The VS method offers benefits in terms of coordination and optimal reference. However, it may face difficulties in designing effective control protocols to increase coordination and consensus within the network (Lu et al., 2012). Moreover, this method relies on a virtual leader which can have a notable influence on control performance.

(b) In graph theory, a MAS is typically depicted as a graph, where individual agents are nodes, and the edges between nodes represent the communication or interaction links between agents (Zheng et al., 2011, Rahmani et al., 2009). While graph theory is a potent mathematical tool for modelling and analyzing diverse systems and it is effective in network expansion (Han et al., 2017), it does come with certain constraints, such as the increasing complexity and analysis challenges when graphs grow in size and intricacy. Additionally, handling the dynamic changes in nodes and edges in real-world applications can pose challenges, which require high communication costs (Han et al., 2017).

(c) For reinforcement learning applied to MAS (Buşoniu et al., 2010, Arel et al., 2010), agents receive reward signals that evaluate the outcomes of their actions in the environment. These rewards guide the agents in making better decisions to maximize their cumulative rewards throughout their interactions. However, RL often requires a large number of interactions with the environment to learn effective policies, which can be impractical or costly in real-world applications. Moreover, the computational complexity increases exponentially with the growth of agent numbers or state-action space (Buşoniu et al., 2010).

(d) Artificial potential field, initially advocated by Khatib (1986), is a virtual force field method inspired by the concept of potential fields in physics. The idea of the APF method is to artificially generate attractive potential fields towards the attractive pole (referred to as 'target' hereafter) and repulsive potential fields around obstacles such that agents can move towards the target and keep away from obstacles. In the context of APF, the 'target' represents the goal or destination that the agent aims to reach, whereas 'obstacle' refers to any object or barrier that the agent needs to avoid (Khatib, 1986, Wolf and Burdick, 2008). For instance, in a highway driving system, the target can be referred to as the desired speed, while obstacles encompass nearby vehicles, hard barriers on roadway edges, and soft boundaries between navigable lanes (Wolf and Burdick, 2008) so that the vehicle can maintain travelling in the desired lane at the desired speed.

Due to its mathematical simplicity, ease of comprehension, and robust real-time and high-efficiency capabilities, APF is extensively used in MAS anti-collision control (Rostami et al., 2019, Duhé et al., 2021) and path planning problems (Sun et al., 2017, Wang et al., 2019). Nevertheless, it is well-known that a significant drawback of the APF is the local minima problem (Park et al., 2001, Chen et al., 2016), especially when dealing with multiple obstacles in two or three-dimensional space. However, in the context of train separation control under VC, this vulnerability can be effectively mitigated within the specific scenario we investigate in this paper, where firstly, train operations only occur on specific tracks, so it can be considered as the motion in a longitudinal space; and secondly, each train under VC in this study is associated with a single dynamic target point and a single obstacle point.

To sum up, the literature review on VC provided above reveals several knowledge gaps to be addressed: (1) A more effective safe train control method under VC with real-time control performance while taking into account a wide range of realistic factors; (2) A safer train separation calculation method under VC to not only avoid train collisions but also prevent triggering emergency braking for the leader; (3) Practical risk factors and parameters in train control under VC with DSM to be considered, and (4) A more realistic representation of train models instead of the mass-point train model.

There is hence the need to define a safe train control method under VC that can not only handle more realistic dynamics of heterogeneous trains operating on realistic tracks based on a homogeneous strip representation of the train model but is also able to consider a train separation with DSM that safely separates trains under VC also in the presence of risk factors such as communication delay, control latencies and sudden emergency braking applications of trains. An APF-based control method is therefore proposed to not only address these mentioned features but also obtain real-time and high-efficiency control performance for trains under VC.

Table 1
Advantages and disadvantages of control algorithms in MAS.

Method	Advantage	Disadvantage
VS (Porfiri et al., 2007, Ren, 2008)	Coordination and optimal control	High difficulty in algorithm design, reliance on the virtual leader,
GT (Zheng et al., 2011, Rahmani et al., 2009)	Simple model structure, powerful mathematical tool, easy to expand	High communication cost, high algorithm complexity in large-scale MAS
RL (Buşoniu et al., 2010, Arel et al., 2010)	Reachability of better performance	High computational complexity in large-scale MAS
APF (Khatib, 1986, Rostami et al., 2019, Duhé et al., 2021)	Mathematical simplicity; robust, real-time and high-efficiency capabilities	Local minima problem

3. Methodology

In this section, first, the problem description and the framework of this paper are introduced in Section 3.1. Second, a homogeneous strip representation of the train model is presented in Section 3.2, based on which the train dynamics and motion model are presented in Section 3.3. In Section 3.4, we introduce a train separation calculation method under VC with DSM based on CBCS. Finally, an improved APF-based train control method under VC is presented in Section 3.5, exploiting the calculated CBCS-based train separation in Section 3.4.

3.1. Problem description

Based on the VC concept, various kinds of scenarios and system structures can be derived. In this paper, we specifically focus on the operational scenario illustrated in Fig. 2, where a train convoy of two trains under VC with train n being the leader and $n+1$ the follower, commences its journey from station A with the initial speed set to zero and an initial separation distance. It is assumed that the follower (train $n+1$) catches up with the leader at a certain point on the route where they start a virtual coupling procedure which leads them to form a virtually connected convoy where they move synchronously with each other until reaching the final station B. Within the convoy, train n transmits its movement information to train $n+1$ using V2V communication. Train $n+1$ employs the received dynamics information (with a communication delay) to calculate its safe separation requirements to the rear of its leader. As for train n, we assume it respects a predetermined speed profile provided by the signalling system.

In this paper, we take into account a realistic rail track with gradients, curves, tunnels and varying speed limits. Additionally, we consider factors like positioning and speed measurement errors of trains. Furthermore, we allow trains n and $n+1$ to have heterogeneous characteristics, including differences in train mass and braking performance. As discussed in the literature, the safe train separation under VC is mostly determined using EBPS. However, we aim to achieve safe and effective control for the journey of train $n+1$ running from station A to station B while keeping a safe train separation with train n by relying on complete braking curve supervision (the service braking curve of train $n+1$ and emergency braking curves of trains n and $n+1$), preventing any triggering of emergency braking actions. The methodology framework of this paper is presented in Fig. 3.

As indicated in Fig. 3, train characteristics and line characteristics are inputs to the APF-based train controller with CBCS. The function to compute the CBCS of the follower train is fed instead by existing risk factors such as communication and control delays, position and speed measurement errors, as well as current train states (i.e. position and speed) from the homogeneous strip model of both the leader and the follower. Specifically the "Complete braking curve calculation" computes two different types of braking distances, hence train separations, both including a dynamic safety margin, namely:

(a) The 'service separation', which is a distance that allows the follower to react to the emergency braking of the leader safely by implementing service braking (the primary braking method during regular train operation). In other words, with the service separation, the follower can come to a full stop safely using service braking (see Fig. 2) when the leader suddenly implements emergency braking.

(b) The 'emergency separation', which represents a critical minimum train separation under emergency braking (see Fig. 2) of the follower. In detail, if the train spacing under VC falls below this threshold, the probability of a collision between trains under VC significantly rises particularly when the leader suddenly implements emergency braking, even if the follower also initiates emergency braking (i.e., the maximum braking capacity achievable by trains).

With the service separation and the emergency separation attached to the rear end of the leader, as illustrated in Fig. 2, we obtain the target and obstacle positions, respectively. These positions, along with the current train states (follower), serve as inputs for the APF-based train controller (see Fig. 3). Subsequently, desired controls are derived from the APF-based train controller and applied to the homogeneous strip train model (follower) taking into account the inertial lag of control. This leads to the updating of train dynamics, generating new inputs for the train separation calculation as well as the APF-based controller.

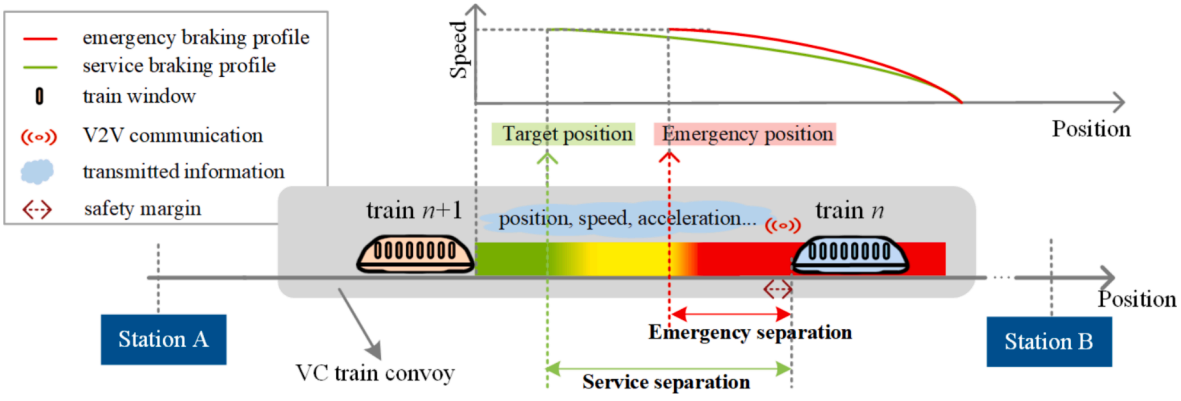

Fig. 2. Operational scenario.

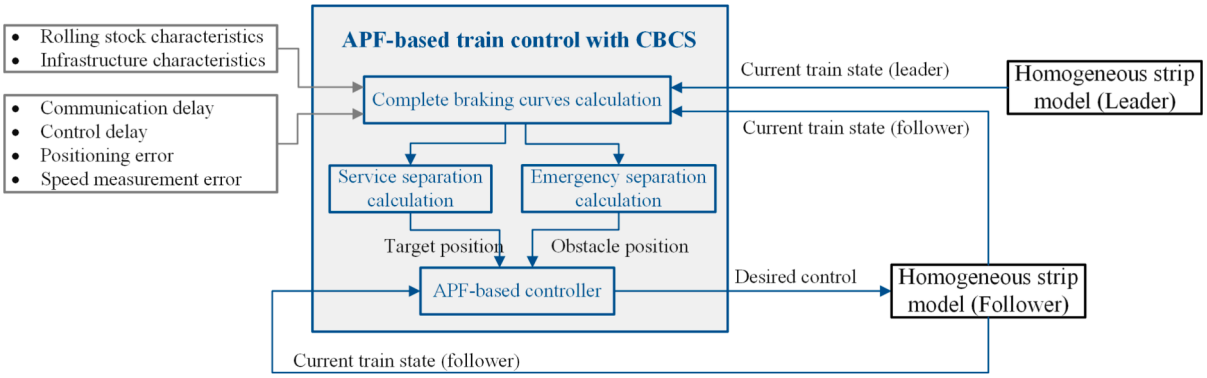

Fig. 3. Methodology framework of APF-based train control under VC with CBCS.

3.2. Homogeneous strip train model

To get a train model with high accuracy of train dynamics, this paper exploits a homogeneous strip (Fan, 2012) modelling method for train representation which divides trains into several segments, each being a homogeneous behavioural train section with the same value of speed, acceleration/ deceleration rate, and jerk, but having its own characteristics including length, curve, and gradient, as shown in Fig. 4. It should be noted that even when considering VC, the train considered in this paper can consist of multiple physically coupled carriages. As mentioned before, under VC signalling where relative braking distances might be shorter than train lengths, it is essential to consider actual train compositions as well as different motion resistances of physically-coupled cars in a train. In particular, train cars can be individually subject to different track gradients or curves even when belonging to the same train.

In Fig. 4(a), $x_n(t)$ and $x_{n,r}(t)$ are the front and rear positions of train n at time t, respectively. $x_{ks,1}(t)$ and $x_{ks,2}(t)$ are the positions of the first and the second knickpoints of the slopes over the track that is occupied by train n at time t, respectively;$h(t)$ is a positive integer denoting the total number of the segments over the train's length at different slopes at time t (e.g. Fig. 4(a) shows the case where $h(t) = 3$); $l_{ks,j}(j = 1, 2, \cdots, h(t))$ is the length of the j^{th} segment of the train; the length of the first train segment is written as $l_{ks,1} = x_n(t) - x_{ks,1}(t)$, the length of the last train segment is defined as $l_{ks,h(t)} = x_{ks,h(t)-1}(t) - x_{n,r}(t)$, and for other train segments, the length is expressed as $l_{ks,j} = x_{ks,j-1}(t) - x_{ks,j}(t)$ where $1 < j < h(t)$;i_j is the gradient of the j^{th} track segment. Based on this homogeneous strip train model, the gradient resistance of train n is defined as

$$R_n^{gr}(t) = \begin{cases} i(x_n(t))M_n g, h(t) = 1 \\ \left(i(x_n(t))l_{ks,1} + \sum_{j=2}^{h(t)} i(x_{ks,j-1}(t))l_{ks,j} \right) \dfrac{M_n}{L_n} g, h(t) \geq 2 \end{cases} \quad (1)$$

where $i(x_n(t))$ is the gradient at position $x_n(t)$ with the gradient positive when the track is uphill and negative when downhill; M_n and L_n are the train mass and length, respectively; g is the gravity acceleration; and $x_{ks,j-1}(t)$ denotes the position of the $(j-1)$th knickpoint of the slopes over the track that is occupied by train n at time t.

In Fig. 4(b),$x_{kc,1}(t)$ and $x_{kc,2}(t)$ are the positions of the two knickpoints of curves within the track that is occupied by the train n at time t, $m(t)$ is a positive integer denoting the total number of the segments over the train length at different curve radii of the track at time t (e.g. Fig. 4(b) shows the case where $m(t) = 3$); $l_{kc,y}$ $(y = 1, 2, \cdots, h(t))$ is the length of the y^{th} segment of the train; the length of

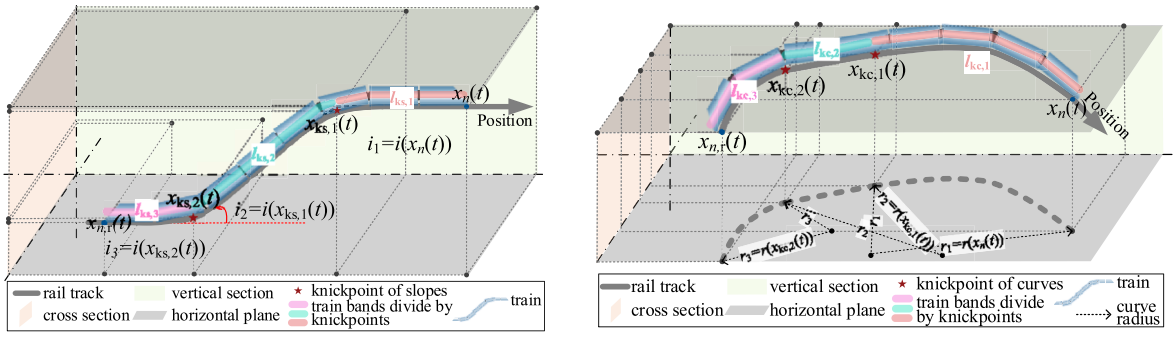

(a) Train on slopes (b) Train on curves

Fig. 4. Homogeneous strip train model.

the first train segment is expressed as $l_{\mathrm{kc},1} = x_n(t) - x_{\mathrm{kc},1}(t)$, the length of the last train segment is defined as $l_{\mathrm{kc},m(t)} = x_{\mathrm{kc},m(t)-1}(t) - x_{n,\mathrm{r}}(t)$, and for other train segments, the length is expressed as $l_{\mathrm{kc},y} = x_{\mathrm{kc},\,y-1}(t) - x_{\mathrm{kc},\,y}(t)$ where $1 < y < m(t)$; and r_y is the curve radius of the y^{th} train segment in a horizontal plane. The curve resistance of train n under homogeneous strip representation can then be written as

$$R_n^{\mathrm{cur}}(t) = \begin{cases} \dfrac{A_c}{r(x_n(t))} M_n g, m(t) = 1 \\ \left(\dfrac{A_c}{r(x_n(t))} l_1 + \sum_{y=2}^{m(t)} \dfrac{A_c}{r\left(x_{\mathrm{kc},y-1}(t)\right)} l_{\mathrm{kc},y} \right) \dfrac{M_n}{L_n} g, m(t) \geq 2 \end{cases} \tag{2}$$

where A_c is an empirical parameter depending on train type; $r(x_n(t))$ is the curve radius of the position $x_n(t)$; and $x_{\mathrm{kc},y-1}(t)$ is the position of the $(y-1)$ th knickpoint of curves over the track that is occupied by the train n at time t.

The influence of in-train forces (or the physical coupler forces) (Sharma and Kumar, 2018), i.e., compression and tension forces, which are the corollary of the sudden contrasts of the longitudinal forces occurring between coaches when the train advances along the track, are not taken into account in this homogeneous strip model. It is beyond the scope of our research, however, it remains to be discussed in further research.

3.3. Train dynamics and motion model

Considering a train convoy under VC consisting of N ($N \geq 2$) trains running on a rail line, the longitudinal train dynamics based on the second Newton's law can be given as (Li et al., 2017, Felez et al., 2019)

$$\begin{cases} \dot{x}_n(t) = v_n(t) \\ \dot{v}_n(t) = a_n(t) = u_n(t) - \dfrac{W_n(t) + R_n(t)}{\rho_n M_n} \\ \dot{u}_n(t) = \dfrac{u_{n,\mathrm{inp}}(t) - u_n(t)}{\tau_{n,\mathrm{a}}} \end{cases} \tag{3}$$

where $x_n(t)$, $v_n(t)$ and $a_n(t)$ are respectively the front position, speed, and acceleration of train n ($n = 1,2,\cdots N$) at time t; $u_{n,\mathrm{inp}}(t)$ and $u_n(t)$ are respectively the desired control of the train and the actual control applied to the train which will be given in Section 3.5; $\dot{u}_n(t)$ refers to the change rate of the actual control; the notations of $\dot{x}_n(t)$ and $\dot{v}_n(t)$ denote the respective time derivatives of distance and speed of train n; $\tau_{n,\mathrm{a}}$ is the inertial delay of train longitudinal dynamics. $W_n(t)$ and $R_n(t)$ are the running resistance and line resistance, respectively; ρ_n denotes the rotating mass factor and can be generally expressed as: $\rho_n = 1 + \gamma_n$, where γ_n is the rotary allowance that is normally regarded as a constant. The effective train mass taking into account the rotational inertia of the rotating components on the train such as wheels and motors (Tian et al., 2019) can be further rewritten as

$$\rho_n M_n = c_n^{\mathrm{e}} m_n^{\mathrm{e}} (1 + \gamma_n^{\mathrm{e}}) + c_n^{\mathrm{t}} m_n^{\mathrm{t}} (1 + \gamma_n^{\mathrm{t}}) \tag{4}$$

where $M_n = c_n^{\mathrm{e}} m_n^{\mathrm{e}} + c_n^{\mathrm{t}} m_n^{\mathrm{t}}$ represents the static train mass; c_n^{e} and c_n^{t} are the numbers of engines and trailers of train n; and m_n^{e}, γ_n^{e} and m_n^{t}, γ_n^{t} are the static mass and rotary allowance of engines and trailers, respectively. $u_n(t)$ and $\dot{u}_n(t)$ are subject to

$$\begin{cases} u_n(t) \in \left[-\beta_{n,\max}(v_n(t)), \dfrac{F_{n,\max}(v_n(t))}{\rho_n M_n} \right] \\ \dot{u}_n(t) \in \left[-\dot{u}_{n,\max}, \dot{u}_{n,\max} \right] \end{cases} \tag{5}$$

where $\beta_{n,\max}(v_n(t))$, $F_{n,\max}(v_n(t))$ and $\dot{u}_{n,\max}$ are the maximum value of the service braking rate, traction effort, and change rate of control of train n, respectively.

Based on the Davis (1926) equation, the running resistance (in Newtons) of the train can be given as

$$W_n(t) = \rho_n M_n \left(A_n + B_n v_n(t) + C_n v_n(t)^2 \right) \tag{6}$$

where $A_n + B_n v_n(t) + C_n v_n(t)^2$ has the unit of N/t, A_n denotes the coefficient encompassing miscellaneous resistances considered to be constant for a specific train such as journal resistance, rolling resistance and track resistance; C_n represents the empirical weight allocated to aerodynamic resistance; and B_n represents the coefficient accounting for residual resistances that are proportionate to the train's speed after deducting the above-mentioned resistances which includes the aerodynamic resistance and journal resistance (Davis, 1926). Commonly, A_n, B_n, and C_n are empirical constant parameters for a specific train but variable according to different types of trains.

While being subjected to the running resistance, trains may also be affected by line resistance which is mostly dependent on the track layout with specific characteristics of the rail tracks. During train operation, the line resistance includes

$$R_n(t) = R_n^{\mathrm{gr}}(t) + R_n^{\mathrm{cur}}(t) + R_n^{\mathrm{tun}}(t) \tag{7}$$

where $R_n^{\mathrm{gr}}(t)$, $R_n^{\mathrm{cur}}(t)$ and $R_n^{\mathrm{tun}}(t)$ are gradient, curve, and tunnel resistance, respectively. $R_n^{\mathrm{gr}}(t)$ and $R_n^{\mathrm{cur}}(t)$ were given in Section 3.2 using the proposed homogeneous strip model. As for tunnel resistance, although the aerodynamic resistance has been included in Equation (6), there is still an additional resistance when a train runs through a tunnel, where the aerodynamic resistance would be different from the situation when the train runs in an open-air environment. Several factors can have an impact on $R_n^{\mathrm{tun}}(t)$ such as the cross-section, the length, and the surface friction coefficient of the tunnel and the train, respectively, and also the most significant factor, the speed of the train. According to Hansen et al. (2017) and Filipović (2015), the additional resistance of a train in a tunnel can be defined as

$$R_n^{\mathrm{tun}}(t) = \left[\frac{(2 + c_n^{\mathrm{e}})}{3} \frac{k_n^{\mathrm{e}}}{A_{\mathrm{t}}^{b_n^{\mathrm{e}}}} + c_n^{\mathrm{t}} \frac{k_n^{\mathrm{t}}}{A_{\mathrm{t}}^{b_n^{\mathrm{t}}}} \right] v_n(t)^2 \tag{8}$$

where k_n^{e}, b_n^{e} and k_n^{t}, b_n^{t} are constant coefficients for engines and trailers of train n, respectively; A_{t} is the cross-section of the tunnel. Practically, tunnel resistance differs in different scenarios such as the process of the train entering and exiting the tunnel, and scenarios like a train meeting another train from the opposite direction (when the two tunnel tubes are not separated by a wall) or following another train in the same direction within the same tunnel tube, which needs to be further considered if we want to get a more precise tunnel resistance. However, this is beyond the scope of this paper.

3.4. Dynamic safe separation calculation model

In VC, the operation of each train is highly dependent on the dynamic information (e.g. position, velocity, acceleration, etc.) transmitted by the leader. This information is crucial for the follower to calculate the safe separation and enable further control actions.

The proposed train separation calculation model includes a dynamic adaptation of the VC safety margin depending on real-time values of safety–critical factors such as train control delays, V2V communication latencies, train position report errors or sudden applications of emergency braking. To this end, the dynamic safety margin defined by Quaglietta et al. (2022) has been considered and embedded in the proposed VC train control model.

In the work by Quaglietta et al. (2022), the DSM is defined as

$$dsm = sm_{\mathrm{pos}} + sm_{\mathrm{com}} + sm_{\mathrm{cont}} + sm_{\mathrm{emer}} + sm_{\mathrm{s}} \tag{9}$$

where sm_{pos}, sm_{com}, sm_{cont}, sm_{emer} and sm_{s} are safety margins concerning risk factors of measurement errors of train positions, V2V communication delays, train control delays, unexpected emergency braking implementations, and external factors which require a constant safety margin to be maintained between two adjacent trains even when they are stationary, respectively (Quaglietta et al., 2022). This paper further develops this DSM model into a CBCS-based dynamic safe train separation calculation model. The calculation in this paper is based on the worst-case assumption that the leader (train n) initiates emergency braking immediately after transmitting its dynamic information and subsequently experiences a V2V communication failure, rendering it unable to transmit any further dynamic information to its follower (train $n+1$), which could potentially account for one of the worst-case situations. However, it is important to acknowledge that there could be worse cases such as train derailment due to uncontrollable external factors or events, which is however beyond the scope of this paper. Besides, it is also assumed that if the waiting time of the follower to receive the next message from its leader exceeds the maximum tolerant V2V communication delay (referred to as $\tau_{\mathrm{com,max}}$ hereafter), then the follower should implement emergency braking. Therefore, to provide the follower with sufficient buffer to react to the potential sudden emergency braking of the leader, the leader is assumed to be decelerating at an emergency braking rate before the follower receives the next message, in other words, minimizing the estimation of the leader's speed to the greatest extent when calculating the train separation requirement during the waiting period of the next V2V communication message from the leader.

We assume that at the time t^*, which denotes any time instant within the maximum tolerant communication delay period the follower has the most recent set of dynamic information (position $x_{n,\mathrm{er}}$, speed $v_{n,\mathrm{er}}$, acceleration a_n, and time t_n) from the leader. The subscript "er" indicates that the variables include measurement errors which will be addressed later in this paper. The follower at time t^*, with speed $v_{n+1,\mathrm{er}}(t^*)$ and position $x_{n+1,\mathrm{er}}(t^*)$, calculates its own complete service braking and emergency braking curves as well as the complete emergency braking curve of its leader to obtain the train separation, i.e. the service separation and emergency separation (see definitions in Section 3.1) required from the follower's front end to the current rear end of the leader, respectively. The current rear end of the leader is determined by the leader together with the train integrity. The CBCS-based dynamic safe train separation calculation model can be written as

$$D_{n+1,\mathrm{CBCS}}(t^*) = \begin{pmatrix} d_{n+1}^{\mathrm{emerg}}(t^*) & d_{n+1}^{\mathrm{serv}}(t^*) \end{pmatrix}^T \tag{10}$$

where $D_{n+1,\mathrm{CBCS}}(t^*)$ denotes the safe train separation requirement of train $n+1$ (as a follower) at time t^* under CBCS, specifically including $d_{n+1}^{\mathrm{emerg}}(t^*)$ and $d_{n+1}^{\mathrm{serv}}(t^*)$ which denote the emergency and service train separations (recall the definitions in Section 3.1), respectively, and are defined as

$$\begin{cases} d_{n+1}^{\text{serv}}(t^*) = \overbrace{RBD_{n+1}^{\text{serv}} + sm_{\text{com}} + sm_{\text{cont}} + sm_{\text{emer}}}^{RBD_{n+1,\text{DSM}}^{\text{serv}}} + \overbrace{sm_{\text{pos}} + sm_{\text{s}}}^{sm_0} \\ d_{n+1}^{\text{emerg}}(t^*) = RBD_{n+1,\text{DSM}}^{\text{emerg}} + sm_0 \end{cases} \tag{11}$$

where sm_0 is a safety margin that includes the train positioning errors in the safety margin sm_{pos} and the constant safety margin sm_{s} from Equation (9); $RBD_{n+1,\text{DSM}}^{\text{serv}}$ denote the CBCS-based Relative Braking Distance (RBD) RBD_{n+1}^{serv} plus sm_{com}, sm_{cont} and sm_{emer} from Equation (9). $RBD_{n+1,\text{DSM}}^{\text{serv}}$ is calculated based on the assumption that the leader takes emergency braking while the follower takes service braking, i.e.

$$RBD_{n+1,\text{DSM}}^{\text{serv}} = \max_{t\in[t^*,t^{\#}]}\left(0, f\left(\xi_{n+1,\text{er}}(t^*), \widetilde{u}_{n+1,\text{wor,serv}}(t^*,t)\right) - f\left(\xi_{n,\text{er}}, \widetilde{u}_{n,\text{wor}}(t^*,t)\right)\right) \tag{12}$$

where function f and its parameters are defined in the following context (see Equations (19), (20) and (35)) in this section. $\widetilde{u}_{n,\text{wor}}(t^*,t) = \left\{\widetilde{u}_{n,\text{wor}}(t^*) | t^* \le \tau \le t\right\}$ and denotes all estimated $\widetilde{u}_{n,\text{wor}}$ over the time range from t^* to t, likewise for $\widetilde{u}_{n+1,\text{wor, serv}}(t^*,t)$. Furthermore, to define a minimum train separation threshold, this paper further extends $RBD_{n+1,\text{DSM}}^{\text{serv}}$ into $RBD_{n+1,\text{DSM}}^{\text{emerg}}$ with the assumption that both the follower and the leader take emergency braking, i.e.

$$RBD_{n+1,\text{DSM}}^{\text{emerg}} = \max_{t\in[t^*,t^{\#}]}\left(0, f\left(\xi_{n+1,\text{er}}(t^*), \widetilde{u}_{n+1,\text{wor,emerg}}(t^*,t)\right) - f\left(\xi_{n,\text{er}}, \widetilde{u}_{n,\text{wor}}(t^*,t)\right)\right) \tag{13}$$

where function f and its parameters are defined in the following context (see Equations (19), (20) and (37)) in this section.

Assuming that according to the complete braking curve calculation, eventually, both trains come to full stops at times $t_{n+1}^{\#}$ and $t_n^{\#}$, respectively, to avoid any potential collisions, the following equation must be satisfied,

$$\forall t \in [t^*, t^{\#}],\ \widetilde{x}_n(t) - L_n - \widetilde{x}_{n+1}(t) \ge sm_0 \tag{14}$$

where $t^{\#} = \max(t_n^{\#}, t_{n+1}^{\#})$, and sm_0 is defined as

$$sm_0 = \left|\varepsilon_{\text{pos},n}\right| + \left|\varepsilon_{\text{pos},n+1}\right| + \varepsilon_{\text{s}} \tag{15}$$

where $|\cdot|$ denotes the absolute value; $\varepsilon_{\text{pos},n}$ and $\varepsilon_{\text{pos},n+1}$ are the positioning errors of train n and $n+1$, respectively. ε_{s} denotes a nominal constant safety margin for trains even when they are stationary. The tilde above a variable denotes the estimated value when assuming braking instead of the actual variable. For instance, $\widetilde{x}_n(t)$ and $\widetilde{x}_{n+1}(t)$ respectively denote the estimated front positions (i.e., positions assuming braking) of train n and $n+1$ at time t from the complete calculated braking curves, and are expressed as

$$\begin{cases} \widetilde{x}_n(t) = x_n(t^*) + s_n(t) \\ \widetilde{x}_{n+1}(t) = x_{n+1}(t^*) + s_{n+1}(t) \end{cases}, t \in [t^*,\ t^{\#}] \tag{16}$$

where $x_n(t^*)$ and $x_{n+1}(t^*)$ are modified train positions which are defined later in Equations (28) and (30), respectively; $s_n(t)$ and $s_{n+1}(t)$ are the estimated braking distances that train n and $n+1$ advances from time t^* to time t ($t \in [t^*,\ t^{\#}]$), respectively. To obtain $s_n(t)$ and $s_{n+1}(t)$, we discretize the train dynamics in Equation (3) and assume a constant train acceleration over time intervals of size Δt such that

$$\begin{cases} v_n(t+\Delta t) = v_n(t) + a_n(t)\Delta t \\ x_n(t+\Delta t) = x_n(t) + v_n(t)\Delta t + \dfrac{1}{2}a_n(t)\Delta t^2 \end{cases} \tag{17}$$

where the time step size Δt will affect the computational accuracy as well as the computation time of the train separation. In general, Δt should be smaller than any of the delays such as communication delays and control delays which are presented in the following sections. Then $s_n(t)$ and $s_{n+1}(t)$ in Equation (16) can be written as

$$s_m(t) \approx \sum_{\tau=t^*}^{t-\Delta t}\left(\widetilde{v}_m(\tau)\Delta t + \frac{1}{2}\widetilde{a}_m(\tau)\Delta t^2\right), t \in [t^*, t^{\#}] \tag{18}$$

where $\widetilde{v}_m(\tau) = v_m(t^*) + \sum_{i=t^*}^{\tau-\Delta t}\widetilde{a}_m(i)\Delta t$, $\widetilde{a}_m(\tau) = \widetilde{u}_m(\tau) - \frac{\widetilde{W}_m(\tau)+\widetilde{R}_m(\tau)}{\rho_m M_m}$, and $\widetilde{u}_m(\tau)$ denote the estimated speed, acceleration, and control of trains at the time τ, respectively, with $m = n, n+1$. $v_m(t^*)$ denotes the modified train speed which is defined in Equations (28) and (30). $s_m(t)$ can be rewritten as

$$\begin{cases} s_n(t) = f\left(\xi_{n,\mathrm{er}}, \widetilde{u}_n(t^*, t)\right) \\ s_{n+1}(t) = f\left(\xi_{n+1,\mathrm{er}}(t^*), \widetilde{u}_{n+1}(t^*, t)\right) \end{cases}, \ t \in [t^*, \ t^{\#}] \tag{19}$$

where f denotes the function computing the braking distance; $\widetilde{u}_n(t^*, t)$ denotes all estimated control of the train over the time range from t^* to t; $\xi_{n+1,\mathrm{er}}(t^*)$ denotes the initial states of train $n+1$ and $\xi_{n,\mathrm{er}}$ denotes the sent dynamics of train n, which can respectively be expressed by

$$\begin{cases} \xi_{n,\mathrm{er}} = \left(x_{n,\mathrm{er}}, v_{n,\mathrm{er}}, u_n\right) \\ \xi_{n+1,\mathrm{er}}(t^*) = \left(x_{n+1,\mathrm{er}}(t^*), v_{n+1,\mathrm{er}}(t^*), u_{n+1}(t^*)\right) \end{cases} \tag{20}$$

Let

$$d(t^*) = x_n(t^*) - L_n - x_{n+1}(t^*) \tag{21}$$

which denotes the separation between train n and $n+1$. Substituting Equations (16), (19) and (21) into Equation (14), then results in

$$\forall t \in [t^*, t^{\#}], \ d(t^*) \geq f\left(\xi_{n+1,\mathrm{er}}(t^*), \widetilde{u}_{n+1}(t^*, t)\right) - f\left(\xi_{n,\mathrm{er}}, \widetilde{u}_n(t^*, t)\right) + sm_0 \tag{22}$$

Let the right-hand side of Equation (22) be denoted by function

$$\delta(t) = \delta\left(\xi_{n,\mathrm{er}}, \xi_{n+1,\mathrm{er}}(t^*), \widetilde{u}_n(t^*, t), \widetilde{u}_{n+1}(t^*, t)\right) \tag{23}$$

To satisfy Equation (22), we obtain:

$$d_{\min}(t^*) = \max_{t \in [t^*, t^{\#}]} \left(\delta\left(\xi_{n,\mathrm{er}}, \xi_{n+1,\mathrm{er}}(t^*), \widetilde{u}_n(t^*, t), \widetilde{u}_{n+1}(t^*, t)\right)\right) \tag{24}$$

where $d_{\min}(t^*)$ denotes the minimum of the service/emergency train separation and will be obtained in the following sections.

3.4.1. Braking curve calculation for the leader of a VC convoy

For train n as a leader, taking into account the velocity measurement and positioning errors, we respectively modify the speed and position of the leader as

$$\begin{cases} v_{n,\mathrm{er,mo}} = v_{n,\mathrm{er}} - \left|\varepsilon_{v,n}\right| \\ x_{n,\mathrm{er,mo}} = x_{n,\mathrm{er}} - \left|\varepsilon_{\mathrm{pos},n}\right| \end{cases} \tag{25}$$

where $\varepsilon_{v,n}$ is the speed measurement error of train n.

Since the follower remains unaware of the operational states of the leader (i.e., accelerating, cruising and decelerating) from the time t_n when the leader sends the message until the time when its next message is received by the follower, there exists a risk of train collision during this "unknown" interval. Therefore, it is necessary to modify the leader's dynamics assuming an emergency braking of the leader.

To modify the acceleration of the leader, considering latencies of V2V communication and dynamic resistances including basic running resistance, gradient resistance, curve resistance, and tunnel resistance, the worst-case $\widetilde{u}_n(t)$ in Equation (18) is defined as

$$\widetilde{u}_{n,\mathrm{wor}}(t) = \begin{cases} -\beta_{n,\mathrm{emerg}}\left(\widetilde{v}_n(t)\right), \mathrm{for} t^* \leq t < t_n^{\#} \mathrm{and} v_{n,\mathrm{er,mo}} > v_{\mathrm{com}} \\ 0, \mathrm{else} \end{cases}, \ t \in [t^*, t^{\#}] \tag{26}$$

where $\beta_{n,\mathrm{emerg}}\left(\widetilde{v}_n(t)\right)$ denotes the emergency braking rate of train n at the estimated speed $\widetilde{v}_n(t)$ which is expressed as $\widetilde{v}_n(t) = v_n(t^* - \tau_{\mathrm{com}}) + \sum_{\tau=t^*-\tau_{\mathrm{com}}}^{t-\Delta t} \widetilde{a}_n(\tau)\Delta t$ with $\widetilde{a}_n(\tau) = \beta_{n,\mathrm{emerg}}\left(\widetilde{v}_n(\tau)\right) - \frac{\widetilde{W}_m(\tau) + \widetilde{R}_m(\tau)}{\rho_m M_m}$; v_{com} denotes the speed threshold under which there may occur a premature stop of the leader within the delay τ_{com}, in other words, if the speed $v_{n,\mathrm{er,mo}}$ is below v_{com}, the leader should be assumed to be already in a full stop at a specific time instant within τ_{com} period. This is out of the concern that if the leader at time $t^* - \tau_{\mathrm{com}}$ (i.e. t_n) has a speed which is very slow (i.e $< v_{\mathrm{com}}$), the leader could have already stopped by the time t^* if it applies emergency braking during the communication delay, which the follower is indeed not able to be aware of. The speed threshold v_{com} is written as

$$v_{\mathrm{com}} = -\sum_{\tau=t^*-\tau_{\mathrm{com}}}^{t^*} \left(-\beta_{n,\mathrm{emerg}}\left(\widetilde{v}_n(t)\right) - \frac{\widetilde{W}_n(\tau) + \widetilde{R}_n(\tau)}{\rho_n M_n}\right)\Delta t \tag{27}$$

where τ_{com} denotes the time difference between the time t^* and time t_n when the leader sent its information (i.e., $\tau_{\text{com}} = t^* - t_n$).

Similar to Equation (26) and on top of Equation (25), the dynamics of train n at time t^* are further modified by

$$\begin{cases} x_n(t^*) = \begin{cases} x_{n,\text{er,mo}} + \zeta_{n,\text{com}}, v_{n,\text{er,mo}} > v_{\text{com}} \\ x_{n,\text{er,mo}} + \zeta^{\#}_{n,\text{com}}, v_{n,\text{er,mo}} \le v_{\text{com}} \end{cases} \\ v_n(t^*) = \begin{cases} v_{n,\text{er,mo}} + v_{\text{com}}, v_{n,\text{er,mo}} > v_{\text{com}} \\ 0, v_{n,\text{er,mo}} \le v_{\text{com}} \end{cases} \end{cases} \tag{28}$$

where $\zeta^{\#}_{n,\text{com}}$ and $\zeta_{n,\text{com}}$ denote the distance that train n decelerates from time $t^* - \tau_{\text{com}}$ to time t^* with and without any premature stop, respectively. According to Equation (18), they can be obtained by

$$\begin{cases} \zeta^{\#}_{n,\text{com}} = \sum_{\tau=t^*-\tau_{\text{com}}}^{t^{\#}_n-\Delta t} \left(\tilde{v}_n(\tau)\Delta t + \frac{1}{2}\tilde{a}_n(\tau)\Delta t^2 \right) \\ \zeta_{n,\text{com}} = \sum_{\tau=t^*-\tau_{\text{com}}}^{t^*-\Delta t} \left(\tilde{v}_n(\tau)\Delta t + \frac{1}{2}\tilde{a}_n(\tau)\Delta t^2 \right) \end{cases} \tag{29}$$

3.4.2. Braking curve calculation for the follower in a VC convoy

For train $n+1$ as a follower, we also consider the speed measurement and positioning errors and modify the speed and position of the follower as

$$\begin{cases} v_{n+1}(t^*) = v_{n+1,\text{er}}(t^*) + |\varepsilon_{v,n+1}| \\ x_{n+1}(t^*) = x_{n+1,\text{er}}(t^*) + |\varepsilon_{\text{pos},n+1}| \end{cases} \tag{30}$$

where $\varepsilon_{v,n+1}$ is the speed measurement error of train $n+1$;

We further incorporate the actual braking process for the follower, as shown in Fig. 5 which involves a series of control delays, including:

The system response delay $\tau_{n+1,A}$, which denotes the time from receiving the command to initiating traction cut-off. This process is within the time interval $[t^*, t_B)$, where $t_B = t^* + \tau_{n+1,A}$;
The traction cut-off delay $\tau_{n+1,B}$, during which the traction force gradually reduces to zero. This process is within the time interval $[t_B, t_C)$, where $t_C = t_B + \tau_{n+1,B}$;
The coasting time $\tau_{n+1,C}$, during which the traction force is zero but the braking force is not yet applied. This process is within the time interval $[t_C, t_D)$, where $t_D = t_C + \tau_{n+1,C}$;
The braking force building delay $\tau_{n+1,D}$, the time required for the braking force to reach the set value ($\tau_{n+1,D}$). This process is within the time interval $[t_D, t_E]$, where $t_E = t_D + \tau_{n+1,D}$.

In practical train operations, these control delays typically fluctuate within certain lower and upper limits, e.g. $\tau_{n+1,A} \in [\underline{\tau}_{n+1,A}, \overline{\tau}_{n+1,A}]$. For safety concerns, we assume that the time delays for the follower are at their upper limits (i.e., $\overline{\tau}_{n+1,A}$, $\overline{\tau}_{n+1,B}$, $\overline{\tau}_{n+1,C}$ and $\overline{\tau}_{n+1,D}$), while the leader has minimal delays (either 0 or infinitesimal). The upper limit of the total control delay is denoted as

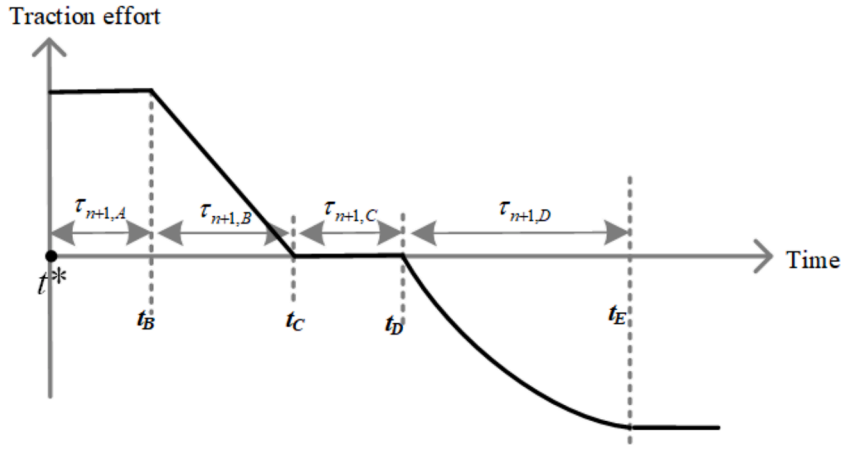

Fig. 5. Braking process breakdown of the follower.

$$\bar{\tau}^{j}_{n+1,\mathrm{con}} = \sum_{i=A}^{D} \bar{\tau}^{j}_{n+1,i},\ j \in \{\mathrm{emerg},\ \mathrm{serv}\} \tag{31}$$

where $\bar{\tau}^{\mathrm{emerg}}_{n+1,\mathrm{con}}$ and $\bar{\tau}^{\mathrm{serv}}_{n+1,\mathrm{con}}$ are total control delays of emergency braking and service braking, respectively. $\bar{\tau}^{\mathrm{emerg}}_{n+1,i}$ and $\bar{\tau}^{\mathrm{serv}}_{n+1,i}$ with $i = A, B, C, D$ denote upper bounds of control delays of different phases (i.e. phases (a)-(b)) for emergency braking and service braking, respectively.

During the response delay phase (a), it is assumed that the follower applies maximum traction using traction force based on its speed-maximum traction characteristic curve $F_{n+1,\max}(v)$ which is a function of speed v. Normally, according to the traction characteristics, at lower speeds, the train operates at a constant maximum traction force. As the speed increases, the train transitions into a constant power phase, during which the traction force decreases hyperbolically. Therefore, the maximal (traction) control in phases (a) and (b) is given by:

$$\widetilde{u}_{n+1,\max}(t) = \frac{F_{n+1,\max}\left(\widetilde{v}_{n+1}(t)\right)}{\rho_{n+1} M_{n+1}},\ t \in [t^{*}, t_C] \tag{32}$$

Therefore, in the worst case, starting at speed $v_{n+1}(t^{*})$, train $n+1$ applies the maximal traction over $\tau_{n+1,A}$ and $\tau_{n+1,B}$ and reaches the maximal speed at the time t_C (referred to as $v^{\max}_{n+1}$ hereafter). In other words, in the worst conditions, the follower accelerates with the maximal control output $\widetilde{u}_{n+1,\max}(t)$ during both phases (a) and (b), and thus at time t_C, its velocity $\widetilde{v}_{n+1}(t_C)$ reaches $v^{\max}_{n+1}$, at which train $n+1$ will be coasting during phase (c).

Furthermore, we also assume a worst case that in phase (d) the braking force applied by the follower remains ineffective until near the end of this phase. In other words, we assume that the follower continues to coast without any output decelerations in the worst-case phase (d), after which the follower reaches service/emergency braking. Therefore, considering both the braking delay and dynamic resistances, the worst-case $\widetilde{u}_{n+1}(t)$ in Equation (18) is written as:

$$\widetilde{u}_{n+1,\mathrm{wor}}(t) = \begin{cases} \widetilde{u}_{n+1,\max}(t), t^{*} \le t \le t_C \\ -\beta_{n+1}\left(\widetilde{v}_{n+1}(t)\right), t_E \le t \le t^{\#}_{n+1} \\ 0, \text{otherwise} \end{cases},\ t \in [t^{*}, t^{\#}] \tag{33}$$

where $\beta_{n+1}\left(\widetilde{v}_{n+1}(t)\right)$ is the braking rate of train $n+1$ with respect to the train speed. According to different braking implementations of train $n+1$, the worst-case $\widetilde{u}_{n+1,\mathrm{wor}}(t)$ in Equation (33) can be divided into

$$\widetilde{u}_{n+1,\mathrm{wor}}(t) = \begin{cases} \widetilde{u}_{n+1,\mathrm{wor,\ emerg}}(t), \mathrm{if}\beta_{n+1}\left(\widetilde{v}_{n+1}(t)\right) = \beta_{n+1,\mathrm{emerg}}\left(\widetilde{v}_{n+1}(t)\right), t_E \le t \le t^{\#}_{n+1} \\ \widetilde{u}_{n+1,\mathrm{wor,\ serv}}(t), \mathrm{if}\beta_{n+1}\left(\widetilde{v}_{n+1}(t)\right) = \beta_{n+1,\mathrm{serv}}\left(\widetilde{v}_{n+1}(t)\right), t_E \le t \le t^{\#}_{n+1} \end{cases},\ t \in [t^{*}, t^{\#}] \tag{34}$$

where $\beta_{n+1,\mathrm{emerg}}\left(\widetilde{v}_{n+1}(t)\right)$ and $\beta_{n+1,\mathrm{serv}}\left(\widetilde{v}_{n+1}(t)\right)$ are the emergency and service braking rate functions with respect to the speed of train $n+1$, respectively. $\widetilde{u}_{n+1,\mathrm{wor,\ emerg}}(t)$ and $\widetilde{u}_{n+1,\mathrm{wor,\ serv}}(t)$ are the worst-case train control output assuming train $n+1$ implements emergency braking and service braking, respectively.

3.4.3. CBCS-based train separation calculation

As presented in Equation (10), the computation of the Complete Braking Curve is performed by taking into account both the emergency and the service separation between leader and follower. The emergency separation is based on the complete emergency braking curves of both the follower and the leader. Substituting Equation (26) and (34) into Equation (24), the emergency separation in Equation (10) is obtained by

$$d^{\mathrm{emerg}}_{n+1}(t^{*}) = \max_{t \in [t^{*}, t^{\#}]}\left(\delta_{\mathrm{emerg}}\left(\xi_{n,\mathrm{er}}, \xi_{n+1,\mathrm{er}}(t^{*}), \widetilde{u}_{n,\mathrm{wor}}(t^{*}, t), \widetilde{u}_{n+1,\mathrm{wor,\ emerg}}(t^{*}, t)\right)\right) \tag{35}$$

where $\delta_{\mathrm{emerg}}(\cdot) = f\left(\xi_{n+1,\mathrm{er}}(t^{*}), \widetilde{u}_{n+1,\mathrm{wor,\ emerg}}(t^{*}, t)\right) - f\left(\xi_{n,\mathrm{er}}, \widetilde{u}_{n,\mathrm{wor}}(t^{*}, t)\right) + sm_0$ (recall Equation (22)) where $sm_0 = \left|\varepsilon_{\mathrm{pos},n,\mathrm{emerg}}\right| + \left|\varepsilon_{\mathrm{pos},n+1,\mathrm{emerg}}\right| + \varepsilon_s$ with $\varepsilon_{\mathrm{pos},n,\mathrm{emerg}}$ denoting the positioning error of train n for the emergency separation calculation, $\widetilde{u}_{n,\mathrm{wor}}(t^{*}, t) = \left\{\widetilde{u}_{n,\mathrm{wor}}(\tau) | t^{*} \le \tau \le t\right\}$ and $\widetilde{u}_{n+1,\mathrm{wor,\ emerg}}(t^{*}, t) = \left\{\widetilde{u}_{n+1,\mathrm{wor,\ emerg}}(\tau) | t^{*} \le \tau \le t\right\}$ where $\widetilde{u}_{n,\mathrm{wor}}(\tau)$ can be obtained by Equation (26) and $\widetilde{u}_{n+1,\mathrm{wor,\ emerg}}(\tau)$ (recall Equation (34)) is rewritten as

$$\widetilde{u}_{n+1,\text{wor, emerg}}(\tau)=\begin{cases}\widetilde{u}_{n+1,\max}(\tau), t^{*}\le\tau\le t_C\\ -\beta_{n+1,\text{emerg}}\left(\widetilde{v}_{n+1}(\tau)\right), t_E\le\tau\le t_{n+1}^{\#}\\ 0, \text{otherwise}\end{cases} \tag{36}$$

where $t^{*}\le\tau\le t$, $t_C=t^{*}+\overline{\tau}_{n+1,A}^{\text{emerg}}+\overline{\tau}_{n+1,B}^{\text{emerg}}$ and $t_E=t^{*}+\overline{\tau}_{n+1,\text{con}}^{\text{emerg}}$ (recall Equation (31)).

The service separation is based on the complete service braking curve of the follower and the emergency braking curve of the leader. Similarly, Substituting Equations (26) and (34) into Equation (24), the service separation in Equation (10) is obtained by

$$d_{n+1}^{\text{serv}}(t^{*})=\max_{t\in[t^{*},t^{\#}]}\left(\delta_{\text{serv}}\left(\xi_{n,\text{er}},\xi_{n+1,\text{er}}(t^{*}),\widetilde{u}_{n,\text{wor}}(t^{*},t),\widetilde{u}_{n+1,\text{wor, serv}}(t^{*},t)\right)\right) \tag{37}$$

where $\delta_{\text{serv}}(\cdot)=f\left(\xi_{n+1,\text{er}}(t^{*}),\widetilde{u}_{n+1,\text{wor,serv}}(t^{*},t)\right)-f\left(\xi_{n,\text{er}},\widetilde{u}_{n,\text{wor}}(t^{*},t)\right)+sm_0$ (recall Equation (22)) where $sm_0=\left|\varepsilon_{\text{pos},n,\text{serv}}\right|+\left|\varepsilon_{\text{pos},n+1,\text{serv}}\right|+\varepsilon_{\text{s}}$ with $\varepsilon_{\text{pos},n,\text{serv}}$ denoting the positioning error of train n for the service separation calculation. $\widetilde{u}_{n+1,\text{wor, serv}}(t^{*},t)=\left\{\widetilde{u}_{n+1,\text{wor, serv}}(\tau)|t^{*}\le\tau\le t\right\}$ where since service braking of the follower is assumed to obtain the service separation, $\widetilde{u}_{n+1,\text{wor, serv}}(\tau)$ (recall the definition in Equation (34)) is rewritten as:

$$\widetilde{u}_{n+1,\text{wor, serv}}(\tau)=\begin{cases}\widetilde{u}_{n+1,\max}(\tau), t^{*}\le\tau\le t_C\\ -\beta_{n+1,\text{serv}}\left(\widetilde{v}_{n+1}(\tau)\right), t_E\le\tau\le t_{n+1}^{\#}\\ 0, \text{otherwise}\end{cases} \tag{38}$$

where $t^{*}\le\tau\le t$, $t_C=t^{*}+\overline{\tau}_{n+1,A}^{\text{serv}}+\overline{\tau}_{n+1,B}^{\text{serv}}$ and $t_E=t^{*}+\overline{\tau}_{n+1,\text{con}}^{\text{serv}}$ (recall Equation (31)).

A calculation example of the proposed CBCS-based train separation calculation method calculating emergency separation is illustrated in Fig. 6, where the complete emergency braking curves of train n and $n+1$ are obtained according to Equations (18), (25)-(34) and (37). Fig. 6 also shows the calculated δ profile (black curve), and the complete train separation profiles during emergency braking of both trains with the follower exploiting an emergency separation at time t^{*} based on EBPS (red solid) and CBCS (red dashed) methods, respectively.

In Fig. 6, the modified speed of the leader is above that of the follower at time t^{*}. Due to the heterogeneous train characteristics including different control delays and braking performances, the follower accelerates to a speed higher than that of the leader and decelerates with a higher braking rate than that of the leader. As a result, as depicted in Fig. 6, the complete train separation between these two trains exhibits an initial increase, followed by a decrease, and ultimately rises again, under which it remains challenging to determine the safe train separation.

To address this problem, we need to ensure that the shortest train separation between these two trains during the entire assumed braking process (i.e., from time t^{*} to $t^{\#}$) can still satisfy the condition in Equation (14). Function $\delta\left(\xi_{n,\text{er}},\xi_{n+1,\text{er}}(t^{*}),\widetilde{u}_{n}(t^{*},t),\widetilde{u}_{n+1}(t^{*},t)\right)$

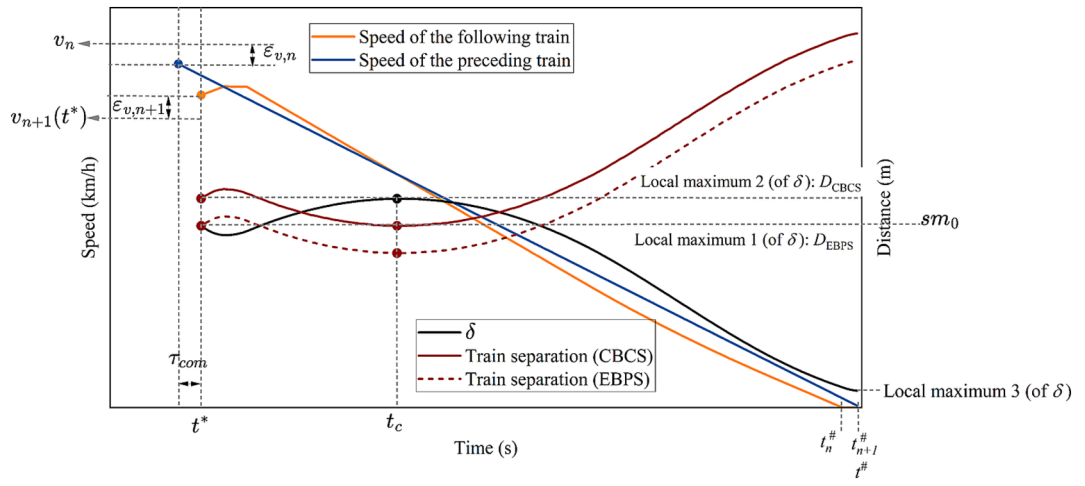

Fig. 6. CBCS-based train separation calculation method.

(referred as function δ hereafter) designed in this paper provides a solution since the global maximum of function δ within the domain $[t^*, t^{\#}]$ represents the minimum requirement of the train separation without triggering emergency braking of the follower (i.e. the emergency separation) according to Equation (35).

Existing EBPS-based train separation calculation methods involve at most two local maxima of the function δ, specifically, both of which are located at the boundaries of the domain of function δ. However, in real train operation, as indicated by the corresponding graph of function δ in Fig. 6, there may exist multiple (>2, typically 3) local maxima for $t \in [t^*, t^{\#}]$, e.g., local maximum 1, 2 and 3, as shown in Fig. 6. In such case, if we employ an EBPS-based train separation, we can only consider up to two boundary points, i.e., local maximum 1 and local maximum 3, while local maximum 2 will be overlooked, which however, can be obtained using the CBCS-based method and represent the actual minimum required emergency separation.

More specifically, take Fig. 6 as an example, the emergency separation determined by EBPS falls below the actual emergency separation calculated by the proposed CBCS method, therefore, in such scenarios, the risk of a train collision significantly increases due to the complete train separation profile infringing on sm_0 under EBPS, especially at time t_c when the train separation reaches its minimum during the entire emergency braking process. Therefore, using a CBCS-based method can prevent potential train collisions or infringements on the emergency separation between two trains under VC by supervising the complete braking process of trains and considering realistic operational factors and train heterogeneities.

Consequently, in this section, the calculation of the emergency and the service train separation under VC addresses numerous practical factors such as measurement errors of train speeds, differences in train traction/braking characteristics, and the complete calculated braking curves influenced by the actual operation conditions. Therefore, in practice, where practical factors are involved, complete predicted braking curves of both the leader and the follower (i.e., CBCS) are needed to obtain the complete function δ. Only then can we locate all the global maxima of the function δ accurately and ultimately identify the correct and safe train separation, i.e., the service and emergency separation. In this way, the risk of train collisions can be mitigated, regardless of any specific braking processes of trains and the presence of risk factors.

3.5. Artificial potential field-based train controller under VC

The Artificial Potential Field (APF) method was proposed by Khatib (1986). The fundamental concept involves constructing an APF that combines an attractive field towards the target and a repulsive field around obstacles. In the context of APF-based control, vehicles are navigated by respecting the gradient of the constructed APF. Specifically, the potential field method metaphorically represents obstacles as elevated peaks characterized by high potential energy values (manifested through steep descents of the repulsive field) on a topographical plane. Conversely, the target point is analogous to a valley marked by a lower potential energy value (exhibiting slow gradient descents of the attractive field). In this way, the vehicle navigates by searching for directions of the decreasing potential energy of APF, enabling collision-free movements. The presence of the attractive and repulsive poles considered in the APF approaches makes it particularly suited to the described need of VC to supervise the complete braking procedure by keeping the safe train separation close to the service separation and far from the emergency separation. In this case, the service separation is employed to create the attractive field, while the emergency separation contributes to generating the repulsive field.

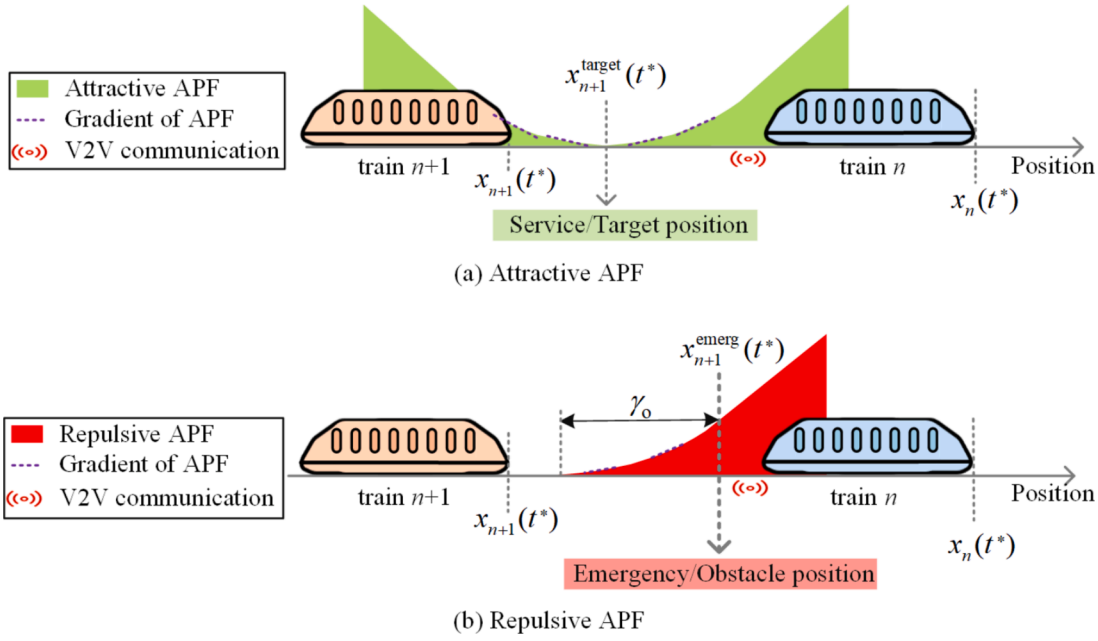

Fig. 7. Diagram of the artificial potential field method in VC.

In this paper, we define the target position to reach as an attractive pole (Fig. 7(a)) and the emergency position that the train should avoid as a repulsive pole (Fig. 7 (b)), i.e., $x_{n+1}^{\text{target}}(t^*)$ is the target and $x_{n+1}^{\text{emerg}}(t^*)$ represents the position of an obstacle in APF of trains under VC at time t^*. They are given by

$$\begin{cases} x_{n+1}^{\text{target}}(t^*) = x_n(t^*) - L_n - d_{n+1}^{\text{serv}}(t^*) \\ x_{n+1}^{\text{emerg}}(t^*) = x_n(t^*) - L_n - d_{n+1}^{\text{emerg}}(t^*) \end{cases} \tag{39}$$

Recall that t^* can be any time instance from the time when the follower receives information from the leader to the time when the follower receives the next message; $x_n(t^*)$ denotes the current rear end of the leader which is determined by the leader. $d_{n+1}^{\text{serv}}(t^*)$ and $d_{n+1}^{\text{emerg}}(t^*)$ are the calculated 'service separation' and 'emergency separation' between trains under VC, respectively (recall the definitions in Section 3.1 and the calculation in Equations (35) and (37)).

Therefore, we generate both attractive APF and repulsive APF artificially to make the train move towards $x_{n+1}^{\text{target}}(t^*)$ while keeping the train away from $x_{n+1}^{\text{emerg}}(t^*)$. The desired control of train $n+1$ at time t^* is then given by

$$u_{n+1,\text{inp}}(t^*) = \frac{F_{\text{attr}}(x_{n+1}(t^*)) + F_{\text{rep}}(x_{n+1}(t^*)) + W_{n+1}(t^*) + R_{n+1}(t^*)}{\rho_{n+1} M_{n+1}} \tag{40}$$

where $F_{\text{attr}}(x_{n+1}(t^*))$ and $F_{\text{rep}}(x_{n+1}(t^*))$ are the attractive force and repulsive force at position $x_{n+1}(t^*)$, resulting from the attractive and repulsive APF functions, respectively, which will be given in Sections 3.5.1 and 3.5.2. The $u_{n+1,\text{inp}}(t^*)$ is used in the train dynamics in Equation (3) to obtain the actual control taking into account the inertial lag of control.

It is important to emphasize that the repulsive pole of the constructed APF in this paper should not be extended to any position further than the emergency position (e.g. the rear end of the leader). This is because, if the follower exceeds the emergency position, there is a serious risk of a collision with the leader in the event of emergency braking by the leader, even if the follower also implements emergency braking (recall the definition of the emergency separation in Section 3.1).

3.5.1. *Artificial attractive and repulsive field*

In VC, the control system drives the follower to move synchronously together with the leader while keeping an expected short separation between each other. In APF, this control feature can be accounted for through an attractive APF, which describes the influence of the targets (i.e., the target position) on the follower to regulate the corresponding APF effort to drive the follower to reach a target separation between its leader.

To this purpose, the attractive APF of train $n+1$ (i.e., the follower) regarding the target position $x_{n+1}^{\text{target}}(t^*)$ [km] is written as

$$U_{\text{attr}}(x_{n+1}(t^*)) = \frac{1}{2} w_{\text{att}} \left(x_{n+1}(t^*) - x_{n+1}^{\text{target}}(t^*) \right)^2 \tag{41}$$

where w_{att} is a gain concerning the train separation. Therefore, the attractive APF effort $F_{\text{attr}}(x_{n+1}(t^*))$ in Equation (40) resulting from the attractive APF function is given by

$$F_{\text{attr}}(x_{n+1}(t^*)) = -\nabla U_{\text{attr}}(x_{n+1}(t^*)) = -w_{\text{att}} \left(x_{n+1}(t^*) - x_{n+1}^{\text{target}}(t^*) \right) \tag{42}$$

where ∇ denotes the gradient of the potential field with respect to position $x_{n+1}(t^*)$ [km].

The obstacle APF describes the influence of the obstacle on the follower, and its final goal is to regulate the corresponding APF effort to keep the follower away from the obstacle position. Usually, the obstacles are depicted by the APF by creating an imaginary mountain of the repulsive field surrounding its physical dimension, as shown in Fig. 7(b), where the coloured area represents the repulsive field of the leader. Basically, in this case, the follower cannot proceed by running through the obstacle due to the presence of an obstacle train in the front. Based on the Gaussian function (Wolf and Burdick, 2008), the following repulsive potential field is introduced

$$U_{\text{rep}}(x_{n+1}(t^*)) = \begin{cases} 0, \text{if} x_{n+1}(t^*) < x_{n+1}^{\text{emerg}}(t^*) - \gamma_o \\ w_o(x_{n+1}(t^*) - x_{n+1}^{\text{emerg}}(t^*)) + U_{\text{rep}}(x_{n+1}^{\text{emerg}}(t^*)), \text{if} x_{n+1}(t^*) > x_{n+1}^{\text{emerg}}(t^*) \\ \int_{-\infty}^{x_{n+1}(t^*)} w_o \exp\left(-\frac{(x_{n+1}(t^*) - x_{n+1}^{\text{emerg}}(t^*))^2}{2{\sigma_o}^2} \right) dx_{n+1}(t^*), \text{otherwise} \end{cases} \tag{43}$$

where γ_o is the maximum impact distance of the obstacle and it is usually considered as a positive constant. Therefore, the obstacle influential surface ranges from position $x_{n+1}^{\text{emerg}}(t^*) - \gamma_o$ to $x_{n+1}^{\text{emerg}}(t^*)$ [km], where at $x_{n+1}^{\text{emerg}}(t^*)$ the repulsive APF reaches its maximum; w_o is the height of the Gaussian function and is a positive weight; $\exp(\bullet)$ denotes the exponential function; σ_o is the standard deviation of the Gaussian function and can be defined as

$${\sigma_o}^2 = -\frac{{\gamma_o}^2}{2\ln\frac{\varepsilon}{w_o}} \tag{44}$$

where ε is a positive constant and significantly smaller than w_o (i.e., $\varepsilon \ll w_o$). Therefore, the repulsive APF effort $F_{rep}(x_{n+1}(t^*))$ in Equation (40) resulting from the repulsive APF function is given by:

$$F_{rep}(x_{n+1}(t^*)) = -\nabla U_{rep}(x_{n+1}(t^*)) = \begin{cases} 0, \text{if} x_{n+1}(t^*) < x_{n+1}^{emerg}(t^*) - \gamma_o \\ -w_o, \text{if} x_{n+1}(t^*) > x_{n+1}^{emerg}(t^*) \\ -w_o \exp\left(-\frac{(x_{n+1}(t^*) - x_{n+1}^{emerg}(t^*))^2}{2{\sigma_o}^2} \right), \text{otherwise.} \end{cases} \tag{45}$$

3.5.2. Dynamic impact distance

As shown in Fig. 8(a), if the target position and the emergency position of the follower are close, then as the train approaches its target, the attractive field experiences a decrease, while the repulsive field experiences a rapid increase. In this situation, the repulsive force derived from the repulsive field is much stronger than the attractive force derived from the attractive field, making it impossible for the train to reach its target point. To address this, as depicted in Fig. 8(b), this paper proposes an improved the APF method by introducing a dynamic impact distance $\gamma_o(t^*)$, defined as

$$\gamma_o(t^*) = x_{n+1}^{emerg}(t^*) - x_{n+1}^{target}(t^*), \text{if} x_{n+1}^{emerg}(t^*) > x_{n+1}^{target}(t^*) \tag{46}$$

which dynamically modifies the impact distance of the emergency position taking into account both the target and emergency positions. In this way, even when the distance between the target and emergency positions decreases to a short distance (e.g. when the speed of the train convoy under VC reaches a low speed), the target position of the follower remains reachable while avoiding the emergency position.

Substituting Equation (46) into Equation (44), Equation (44) can be rewritten as

$${\sigma_o}^2(t^*) = -\frac{{\gamma_o}^2(t^*)}{2\ln\frac{\varepsilon}{w_o}} = -\frac{\left(x_{n+1}^{emerg}(t^*) - x_{n+1}^{target}(t^*)\right)^2}{2\ln\frac{\varepsilon}{w_o}} \tag{47}$$

where $\sigma_o(t^*)$ is the standard deviation of the Gaussian function at time t^*, which can be generated dynamically according to the dynamic changes in the values of $x_{n+1}^{target}(t^*)$ and $x_{n+1}^{emerg}(t^*)$ (i.e., the target and the obstacle position). Therefore, the repulsive APF effort in

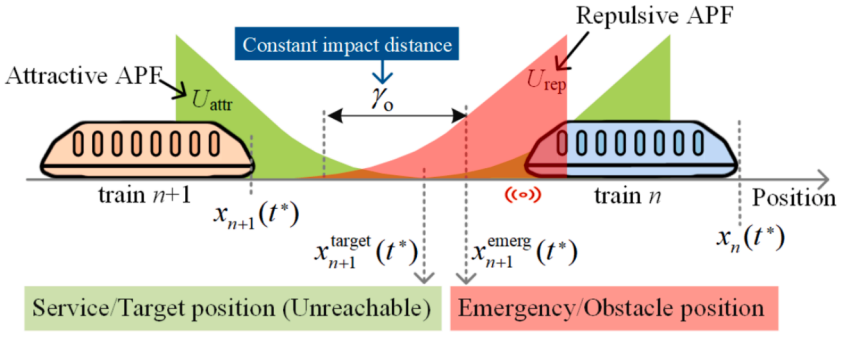

(a) APF with constant impact distance

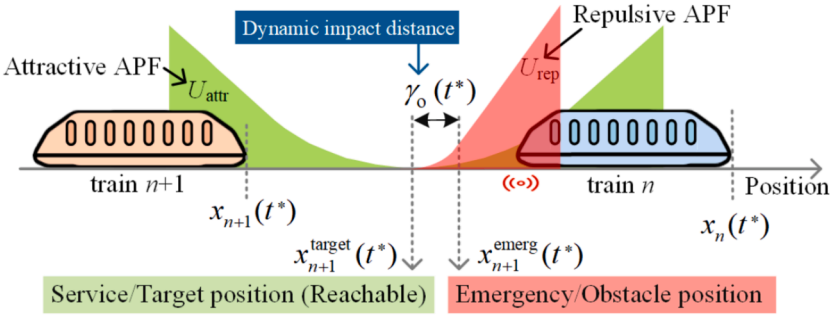

(b) Improved APF with dynamic impact distance

Fig. 8. Comparison of APF between exploiting constant and dynamic impact distance.

Equation (45) can be rewritten as

$$F_{\text{rep}}(x_{n+1}(t^*)) = \begin{cases} 0, \text{if } x_{n+1}(t^*) < x_{n+1}^{\text{target}}(t^*) \\ -w_o, \text{if} x_{n+1}(t^*) > x_{n+1}^{\text{emerg}}(t^*) \\ -w_o \exp\left(-\dfrac{(x_{n+1}(t^*) - x_{n+1}^{\text{emerg}}(t^*))^2}{2{\sigma_o}^2(t^*)}\right) = -w_o \exp\left(\dfrac{(x_{n+1}(t^*) - x_{n+1}^{\text{emerg}}(t^*))^2}{(x_{n+1}^{\text{emerg}}(t^*) - x_{n+1}^{\text{target}}(t^*))^2} \ln\dfrac{\varepsilon}{w_o}\right), \text{ otherwise.} \end{cases} \tag{48}$$

4. Experiments and results

4.1. Case study description

The proposed APF-based train control algorithm for supervising the complete train braking curves and the dynamic safety margin has been validated through simulations with real-world operational data from a high-speed railway corridor in China. Specifically, the railway corridor from station Hengyang East (HYE) to Leiyang West (LYW) is considered, covering a distance of 20.2 km. Fig. 9 illustrates the gradient and curve radius of the high-speed corridor. Within this corridor, there are also two tunnels covering from 15.2 km to 15.6 km and from 18.2 km to 18.4 km, respectively.

The main objective of the experimental design is to assess the performance of the developed APF-based train control for different combinations of heterogeneous trains in a VC convoy as well in the presence of risk factors such as response delays in signalling and/or communication systems. A comparison is also made between the End Braking Point Supervision and the Complete Braking Curve Supervision to assess the corresponding impacts on the control indications received by the follower. The experiments consider two trains having heterogeneous rolling stock characteristics following each other in a VC convoy. The initial separation at departure between the two trains is set to 250 m. In the VC train convoy, the leader is assumed to move according to the planned speed profile on the experimental corridor (illustrated in Fig. 9) which includes running time allowances enabling the train to cruise at speeds lower than the max track speed limits. The follower is instead assumed to be virtually coupled to the leader and move synchronously with it by following speed controls provided by the developed APF-based algorithm.

The traction and braking characteristics of the CRH6A (China Railway High-speed 6 A) train are given in Table 2 where $F_{\max}(v)$ denotes the maximum traction effort of the CRH6A train (recall $F_{n,\max}(v_n(t))$ in Equation (5)).

Other input parameters are detailed in Table 3 where CRH6A-1 and CRH6A-2 are the two variants of the same rolling stock of CRH6A, with different characteristics corresponding to the two heterogeneous experimental trains exploited in our experiments. Specifically, CRH6A-1 is the original rolling stock of the intercity Electric Multiple Units (EMUs) of CRH6A, while it is assumed that CRH6A-2 has 25 % lower braking capability than CRH6A-1.

The coefficients of w_{att}, w_o and ε concerning the APF function are fine-tuned manually through experiments. To determine the optimal attractive APF weight (w_{att}), the weight w_{att} is calibrated to achieve the shortest convergence time of the leader to reduce separation deviation (given initial separation deviations) between the actual and the service separations. Determination of the optimal repulsive APF weight (w_o) involves emergency braking tests of the leader at different speeds from 0 to 200 km/h. The weight w_o is calibrated to identify the optimal control performance of the follower preventing infringements of the emergency separation using service braking (i.e. the follower avoids approaching the emergency position even when applying service braking in response to the sudden emergency braking of the leader) while simultaneously minimizing fluctuations in the change rate of follower's control. The weight ε, as presented in Section 3.5.1, should satisfy the condition $\varepsilon \ll w_o$. All calibration processes are conducted under different combinations of trains in the VC convoy, specifically the combination CRH6A-1/CRH6A-2 with CRH6A-1 as the follower and CRH6A-2 as the leader, and the combination CRH6A-2/CRH6A-1 with CRH6A-2 being the follower and CRH6A-1 the leader.

The objective of the experiments is to test the performance of the proposed APF-based train control algorithm for different com-

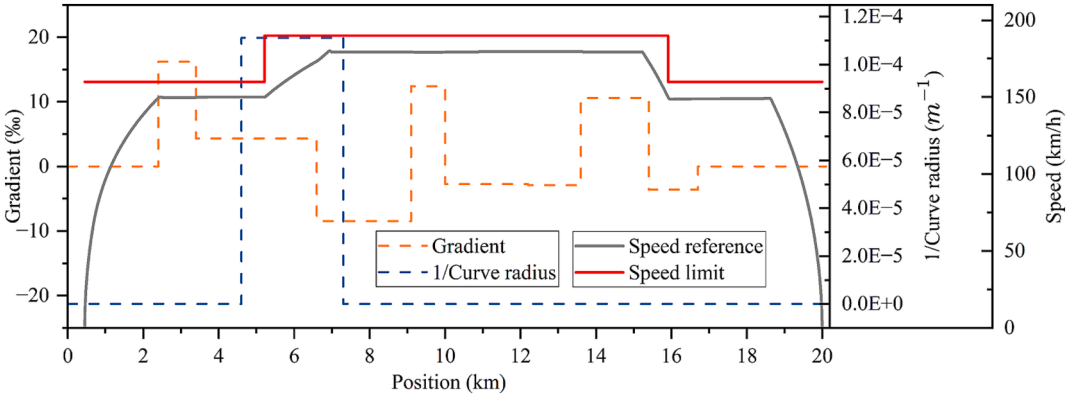

Fig. 9. Experimental line characteristics and speed reference.

Table 2
Braking characteristics of CRH6A trains.

Speed (v) (km/h)	Service braking rate (m/s^2)	Emergency braking rate (m/s^2)	Speed (v) (km/h)	$F_{\max}$(N)
$v \in [0,5]$	0.8654	0.999	$v \in (0,60]$	296,010
$v \in (5,20]$	$0.0203071v + 0.7639$	$0.8820 + 0.0234v$	$v \in (60,200]$	$5161200/v$
$v \in (20,70]$	1.17	1.35		
$v \in (70,118]$	$-0.0017749v + 1.2942$	$1.3879 - 0.0005418v$		
$v \in (118,200]$	$-0.002231v + 1.348$	$1.8752 - 0.0046716v$		

Table 3
Parameters of experiments.

Parameter	Notation	Value
Train length	L_n, L_{n+1}	201 [m]
Numbers of engines and trailers	c_n^e, c_{n+1}^e; c_n^t, c_{n+1}^t	4
Mass of engines (CRH6A-1)	m_n^e, m_{n+1}^e	190 [t]
Mass of engines (CRH6A-2)		218 [t]
Mass of trailers (CRH6A-1)	m_n^t, m_{n+1}^t	180 [t]
Mass of trailers (CRH6A-2)		208 [t]
Rotary allowance of engines	γ_n^e, γ_{n+1}^e	0.1 [N^{-1}]
Rotary allowance of trailers	γ_n^t, γ_{n+1}^t	0.05 [N^{-1}]
Actuator lag of train	$\tau_{n,a}$, $\tau_{n+1,a}$	0.5 [s]
Total control delay	$\overline{\tau}_{n+1,con}^{emerg}$, $\overline{\tau}_{n+1,con}^{serv}$	1.5, 1 [s]
Response delay	$\overline{\tau}_{n+1,A}$	$\overline{\tau}_{n+1,con}/6$
Traction cut-off delay	$\overline{\tau}_{n+1,B}$	$\overline{\tau}_{n+1,con}/3$
Coasting delay	$\overline{\tau}_{n+1,C}$	$\overline{\tau}_{n+1,con}/6$
Braking implementation delay	$\overline{\tau}_{n+1,D}$	$\overline{\tau}_{n+1,con}/3$
Coefficients of basic resistance	A_n, B_n, $C_n (m = n, n+1)$	5.4 [N/t], 9.8e-3 [N/t/km.h^{-1}], 1.63e-3 [N/t/km.h^{-2}]
Cross-section of tunnels	A_t	100.11 [m^2]
Coefficients of tunnel resistance	k_m^e, k_m^t, b_m^e, $b_m^t (m = n, n+1)$	1140, 662, 1.48, 1.75
Speed measurement error	$\varepsilon_{v,n}$, $\varepsilon_{v,n+1}$	0.5 [km/h]
Positioning error	$\varepsilon_{pos,m,emerg}$, $\varepsilon_{pos,m,serv}$, $\varepsilon_{pos,m} (m = n, n+1)$	7.5, 5, 5 [m]
Constant safety margin	ε_s	5 [m]
Maximum change rate of control	$\dot{u}_{n,max}$, $\dot{u}_{n+1,max}$	0.8 [m/s^3]
Maximum communication delay	$\tau_{com,max}$	0.2 [s]
Time step size	Δt	0.1 [s]
Attractive APF weight	w_{att}	1e7
Repulsive APF weight	w_o	4e5
Nominal positive constant	ε	$w_o/1000$

binations of heterogeneous trains under VC with different Dynamic Safety Margins (DSMs). Additionally, the dynamic impact distance of the emergency position (i.e., the repulsive pole in the APF) proposed in this paper is compared with a constant impact distance of 10 m as defined in the literature (Guo and Li (2023)). For clarity, cases employing a constant impact distance are denoted with the suffix "_c" at the end. All case studies are detailed in Table 4, where D_{appr}, D_{EBPS}, and D_{CBCS} are given in Table 5 and defined as:

D_{appr}, refers to an approximate calculation method of train separation with DSM taking into account only the difference of total braking distances of trains by referring to an EBPS-based train separation, using flat tracks and without including any risk factor;
D_{EBPS}, refers to an EBPS-based train separation with DSM and considers realistic track characteristics and risk factors, as illustrated in Section 2.2.

Table 4
Simulation setting of cases.

Case	DSM	The follower	The leader	Impact distance of the repulsive APF
D_{appr}_CRH6A-1/CRH6A-2	D_{appr}	CRH6A-1	CRH6A-2	Dynamic
D_{appr}_CRH6A-2/CRH6A-1	——	CRH6A-2	CRH6A-1	Dynamic
D_{EBPS}_CRH6A-1/CRH6A-2	D_{EBPS}	CRH6A-1	CRH6A-2	Dynamic
D_{EBPS}_CRH6A-2/CRH6A-1	——	CRH6A-2	CRH6A-1	Dynamic
D_{CBCS}_CRH6A-1/CRH6A-2	D_{CBCS}	CRH6A-1	CRH6A-2	Dynamic
D_{CBCS}_CRH6A-2/CRH6A-1	——	CRH6A-2	CRH6A-1	Dynamic
D_{EBPS}_CRH6A-1/CRH6A-2_c	D_{EBPS}	CRH6A-1	CRH6A-2	Constant
D_{EBPS}_CRH6A-2/CRH6A-1_c	——	CRH6A-2	CRH6A-1	Constant
D_{CBCS}_CRH6A-1/CRH6A-2_c	D_{CBCS}	CRH6A-1	CRH6A-2	Constant
D_{CBCS}_CRH6A-2/CRH6A-1_c		CRH6A-2	CRH6A-1	Constant

Table 5
Definitions of different DSM.

DSM	Calculation Method	Separation	Definition
D_{appr}	EBPS (with flat tracks and no risk factors)	Service	$\max\left(sm_0, \frac{v_{n+1}(t)^2}{2\beta_{n+1,\text{serv}}(v_{n+1}(t))} - \frac{v_n(t)^2}{2\beta_{n,\max}}\right)$
		Emergency	$\max\left(sm_0, \frac{v_{n+1}(t)^2}{2\beta_{n+1,\text{emerg}}(v_{n+1}(t))} - \frac{v_n(t)^2}{2\beta_{n,\max}}\right)$
D_{EBPS}	EBPS	Service	$\max\left(sm_0, \delta_{\text{serv}}\left(\xi_{n,\text{er}}, \xi_{n+1,\text{er}}(t^*), \widetilde{u}_{n,\text{wor}}(t^*, t^\#), \widetilde{u}_{n+1,\text{wor, serv}}(t^*, t^\#)\right)\right)$
		Emergency	$\max\left(sm_0, \delta_{\text{emerg}}\left(\xi_{n,\text{er}}, \xi_{n+1,\text{er}}(t^*), \widetilde{u}_{n,\text{wor}}(t^*, t^\#), \widetilde{u}_{n+1,\text{wor, emerg}}(t^*, t^\#)\right)\right)$
D_{CBCS}	CBCS	Service	$\max_{t\in[t^*,t^\#]}\left(\delta_{\text{serv}}\left(\xi_{n,\text{er}}, \xi_{n+1,\text{er}}(t^*), \widetilde{u}_{n,\text{wor}}(t^*, t), \widetilde{u}_{n+1,\text{wor, serv}}(t^*, t)\right)\right)$
		Emergency	$\max_{t\in[t^*,t^\#]}\left(\delta_{\text{emerg}}\left(\xi_{n,\text{er}}, \xi_{n+1,\text{er}}(t^*), \widetilde{u}_{n,\text{wor}}(t^*, t), \widetilde{u}_{n+1,\text{wor, emerg}}(t^*, t)\right)\right)$

D_{CBCS}, uses instead a CBCS-based train separation with DSM to take into account the supervision of the complete train braking process, realistic track characteristics and operational risk factors.

To present the preliminary findings regarding the emergency separation that considers the most safety–critical train separation requirement, we conducted comparative experiments to calculate different emergency separations employing three different calculation methods with different DSMs (as defined in Table 5): D_{appr}, D_{EBPS}, and D_{CBCS}, respectively. In these experiments, all methods were fed with the same set of speed profiles of the leader (CRH6A-2) and the follower (CRH6A-1), depicted in Fig. 10 by the solid blue and orange lines, respectively. Trains are running on the experimental line illustrated in Fig. 9. The results for the different emergency separations are shown in Fig. 10. As the emergency separation using the proposed CBCS method fully supervises the complete train braking process while taking into account realistic track characteristics and operational risk factors, the emergency separation in D_{CBCS} is considered as the benchmark (the solid red line in Fig. 10). Therefore, results of either D_{appr} or D_{EBPS} are considered incorrect and risky if their emergency separations infringe the emergency separation in D_{CBCS}, i.e., when the solid or dotted purple lines in Fig. 10 fall below the solid red line. According to Fig. 10, the emergency separations calculated using the approximate method and the EBPS method frequently falls aggressively below the benchmark (the emergency separation in D_{CBCS}). Additionally, the emergency separation in D_{appr} exhibit rapid fluctuations in response to the changes in the speed profiles of the leader and the follower.

4.2. Computation time

The computation time of the proposed APF-based train control under Complete Braking Curve Supervision is analyzed in this section to determine the optimal calculation time step size. The basic experimental parameters respect the settings in Section 4.1. The simulation experiments are conducted using PyCharm 2019.3.3 (Professional Edition), which runs on Windows 11 with a 64-bit operating system and is powered by a 12th Gen Intel(R) Core(TM) i7-12700H processor.

Fig. 11 presents contour plots with colour fill, illustrating the computation time of the train control under CBCS with different calculation time step sizes (i.e. Δt) of 0.5 s, 0.1 s and 0.05 s, respectively. In each plot, the colours represent the computation time for different speed combinations of the follower and the leader, both ranging from 0 to 200 km/h. The corresponding computation time can be identified using the colour bar on the right side of each plot. For instance, in Fig. 11(c) where $\Delta t = 0.05$ s, the computation time

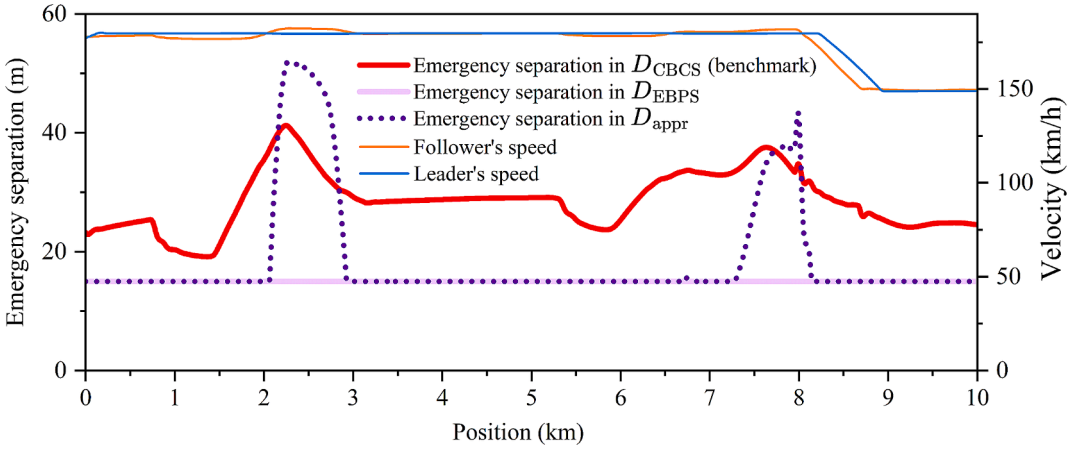

Fig. 10. Comparison of emergency separations with different DSMs.

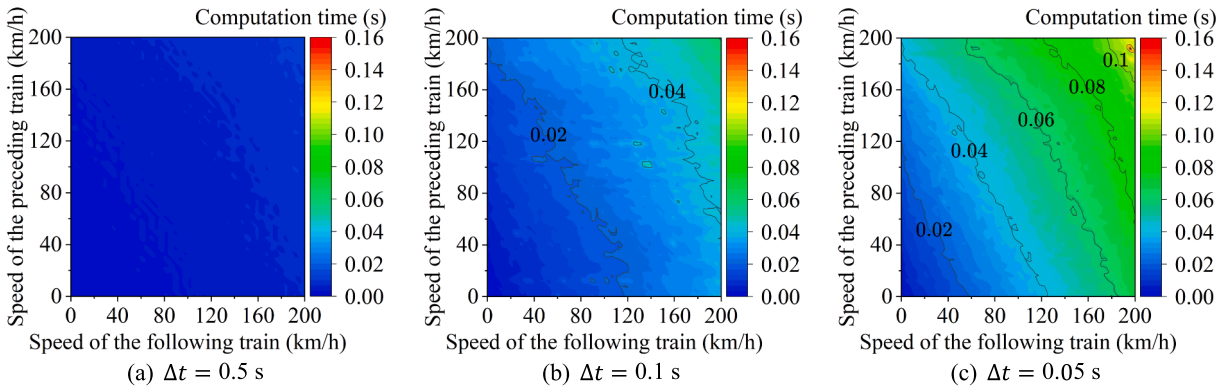

Fig. 11. Comparison of the computation time under different time step sizes.

is 0.08 s when the leader and the follower both are at the speed of 160 km/h.

As depicted in Fig. 11, an increase in train speeds or a decrease in the calculation time step Δt results in higher computation time. Comparing Fig. 11(a), (b), and (c), the most significant increase in computation time is observed when $\Delta t = 0.05$ s in Fig. 11(c) where the computation time can exceed 0.1 s. Conversely, the most efficient computation time is observed in Fig. 11(a) with $\Delta t = 0.5$ s. For train control systems where the train control period (Ma et al., 2016) (i.e. the time interval to complete computing and generating the next control indication for trains) is designed as 200 ms, all the computation time in Fig. 11 meets the real-time train control requirement. However, for those trains whose control period is 100 ms, the computation time may fail to meet the real-time train control requirement particularly when Δt is equal to (or less than) 0.05 s and trains are at higher speeds (e.g. 180 km/h), according to Fig. 11(c).

To study the effect of time step size on the computation accuracy of the safe train separation, we compare the errors obtained for different Δt. Given that a shorter Δt contributes to higher computation accuracy, the computation results with $\Delta t = 0.05$ s are therefore considered as the reference. Then, a comparative analysis of the computation errors in the service separation (i.e. d_{n+1}^{serv}) between $\Delta t = 0.5$ s and $\Delta t = 0.1$ s is conducted to determine the appropriate Δt. This analysis also takes int account all speed combinations of the follower and the leader with speeds both ranging from 0 to 200 km/h. In other words, the comparison between $d_{n+1}^{\text{serv}}|_{\Delta t=0.5} - d_{n+1}^{\text{serv}}|_{\Delta t=0.05}$ and $d_{n+1}^{\text{serv}}|_{\Delta t=0.1} - d_{n+1}^{\text{serv}}|_{\Delta t=0.05}$ is illustrated in Fig. 12, where $d_{n+1}^{\text{serv}}|_{\Delta t=0.5}$ denotes the computation result of the service separation when Δt equals 0.5 s.

The results depicted in Fig. 12(a) illustrate that when $\Delta t = 0.5$ s, the computation error of the service separation (referenced to $\Delta t = 0.05$ s), i.e. $d_{n+1}^{\text{serv}}|_{\Delta t=0.5} - d_{n+1}^{\text{serv}}|_{\Delta t=0.05}$, can extend to several meters, particularly as the speed of the follower increases. While with $\Delta t = 0.1$ s, the computation error (i.e. $d_{n+1}^{\text{serv}}|_{\Delta t=0.1} - d_{n+1}^{\text{serv}}|_{\Delta t=0.05}$) in Fig. 12(b) can be within one meter, covering the whole range of the speeds of trains. Therefore, taking into account factors of train speeds, computation time and error, Δt is adopted as 0.1 s hereafter.

4.3. Control performance analysis

In this section a comparative assessment of the proposed APF-based control model is performed among the three considered

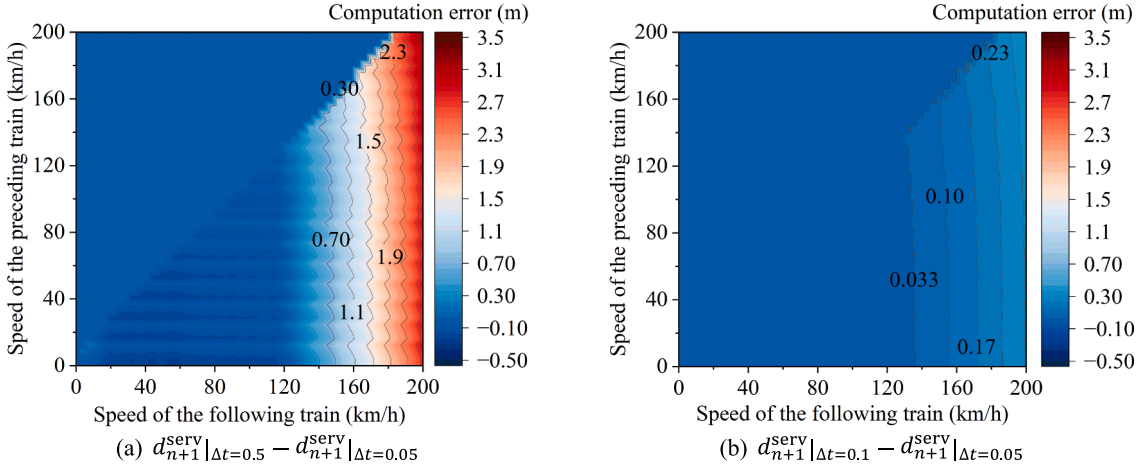

Fig. 12. Comparison of the computation error of d_{n+1}^{serv}.

different braking supervision cases (i.e. D_{appr}, D_{EBPS} and D_{CBCS} given in Table 5) and for each of the two follower-leader sequences in the VC convoy (i.e., CRH6A-1/CRH6A-2 and CRH6A-2/CRH6A-1 in Table 4). The dynamic impact distance of the emergency position proposed in this paper is also compared with a constant impact distance.

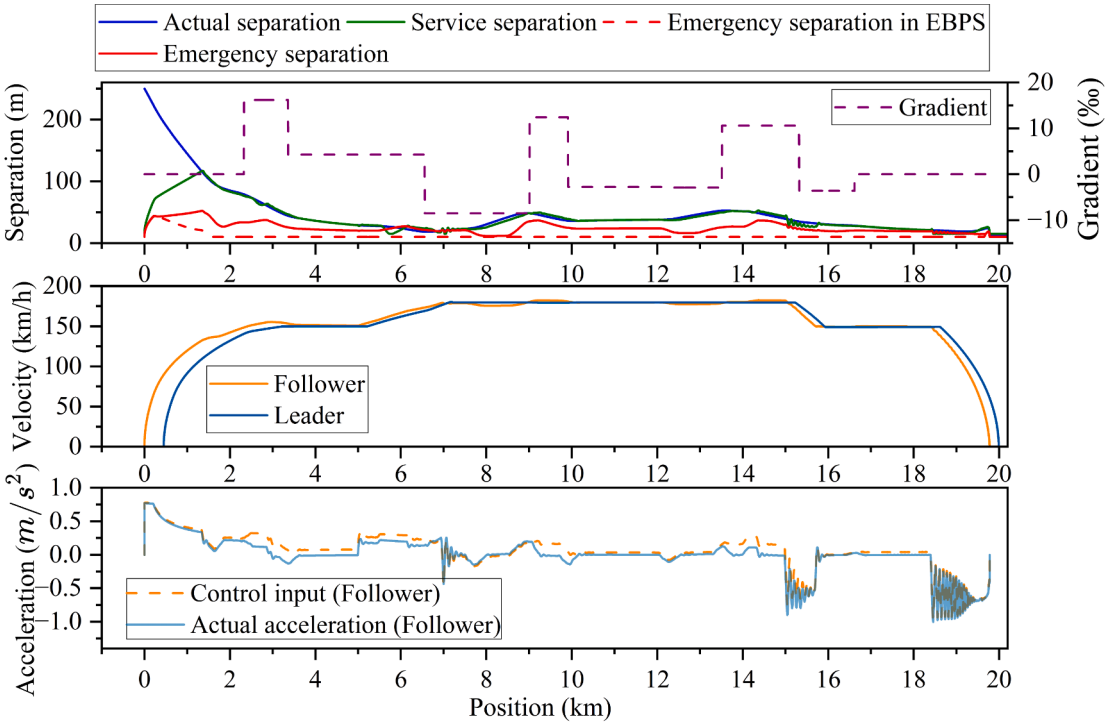

(a) Case D_{EBPS}_CRH6A-1/CRH6A-2 showing emergency separation infringements and unstable control

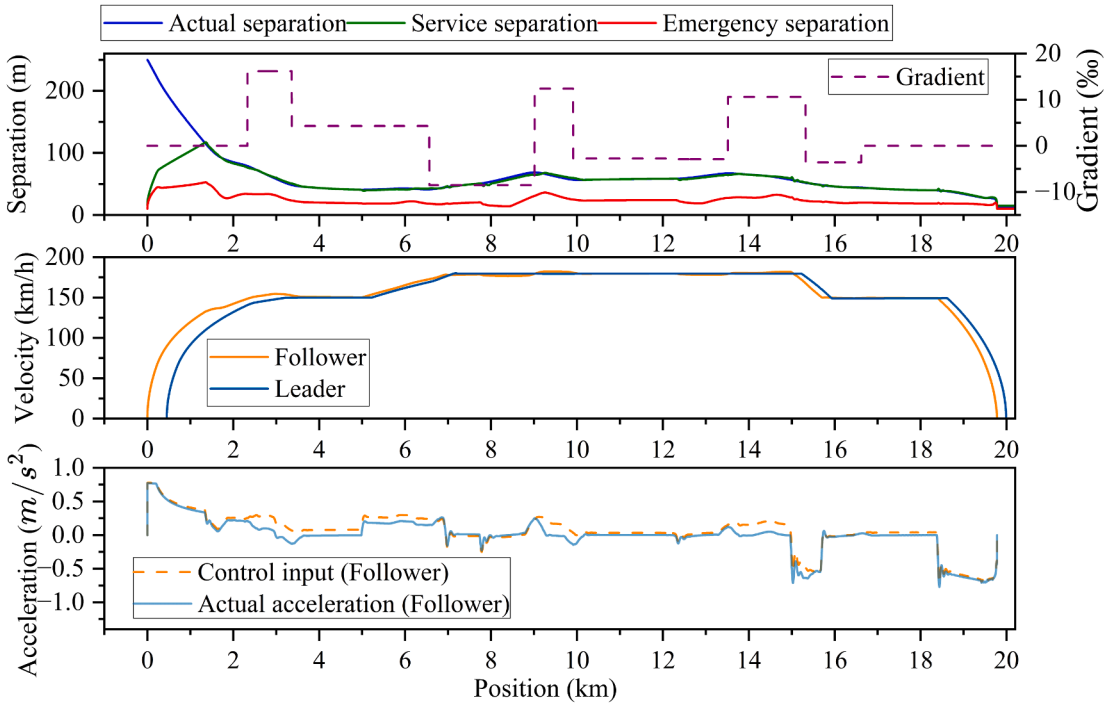

(b) Case D_{CBCS}_CRH6A-1/CRH6A-2 showing compliance with emergency separation and stable control

Fig. 13. Separation, speed, and acceleration profiles.

The assessment is made based on several Key Performance Indicators (KPIs), namely:

Collision (Yes/No): whether the front end of the follower infringes the rear end of the leader
Average train separation (s_{ave}): the average of the actual train separation between the front end of the follower and the rear end of the leader across the whole experimental railway corridor.
Maximum negative separation deviation ($d_{ne,max}$): the maximum negative deviation between the actual train separation and the calculated service separation across the whole corridor, indicating the maximum distance by which the actual position of the follower surpasses its target position leading the follower to approach the emergency position). It should be noted that the negative separation deviation does not imply train collisions but indicates the distance that the follower exceeds the target position.
Overall time the maximum change rate of control is reached ($t_{\dot{u}\_max}$): the total cumulative time of the train control reaching the maximum change rate of control, either positive ($\dot{u}_{n,max}$) or negative ($-\dot{u}_{n,max}$), within the whole corridor.
Number of infringements (n_{in}): the number of times the emergency separation is infringed within the whole corridor, triggering an emergency brake in real-world VC train operations.

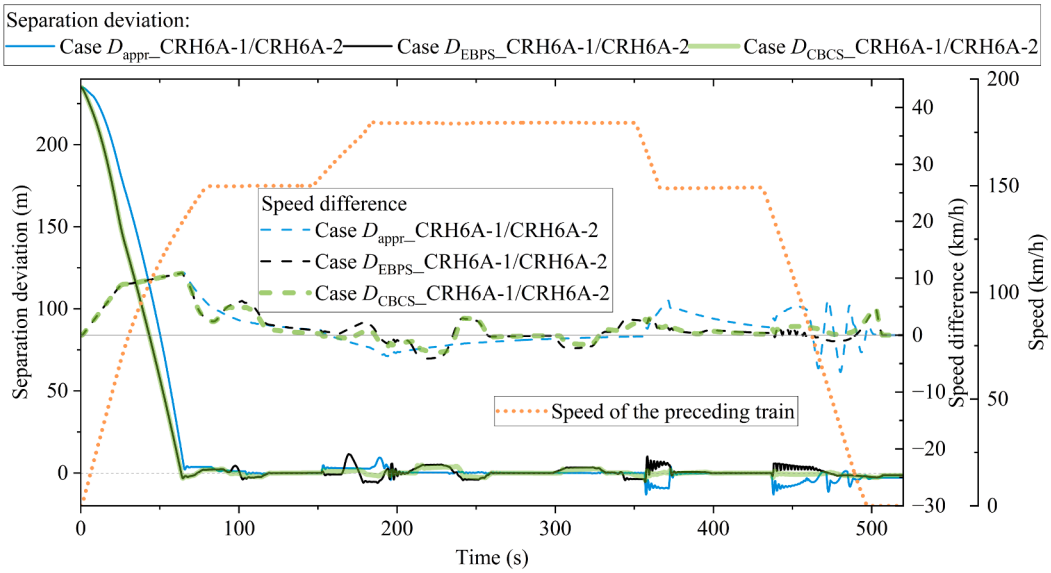

(a) The follower: CRH6A-1; Leader: CRH6A-2

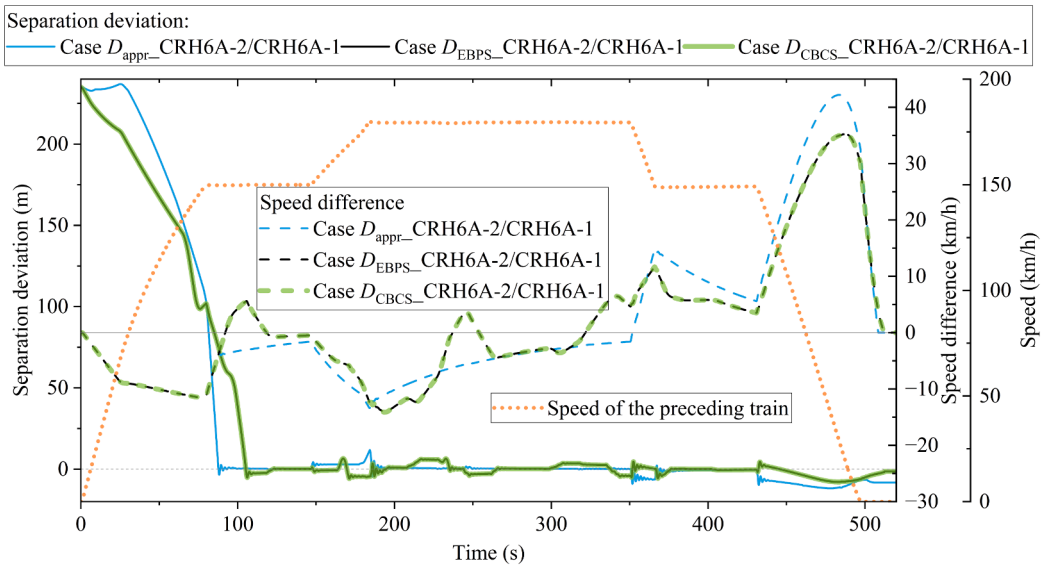

(b) Follower: CRH6A-2; Leader: CRH6A-1

Fig. 14. Separation deviations and speed differences.

Overall infringement duration of emergency separation (t_{in}): the total cumulative time during which the follower infringes the emergency separation (i.e., exceeds the emergency position) within the entire corridor. It should be noted that collisions may occur when the follower infringes the emergency position and meanwhile, the leader takes a sudden emergency braking.
Maximum infringement distance ($d_{in,max}$): the maximum distance the follower exceeds the emergency position within the whole corridor.
Maximum negative emergency separation error ($e_{ne,max}$): the maximum negative error between the emergency separation calculated with D_{appr} (or D_{EBPS}) and that derived from the CBCS method, which is considered as the benchmark.

Fig. 13 depicts the separation, velocity, and acceleration profiles versus position derived from simulation results of two cases: Case D_{EBPS}_CRH6A-1/CRH6A-2 as presented in Fig. 13(a), and Case D_{CBCS}_CRH6A-1/CRH6A-2 illustrated in Fig. 13(b), which utilize D_{EBPS} and D_{CBCS}, respectively. These result diagrams, as well as the result diagrams of the other cases in Table 4, i.e. Cases D_{appr}_CRH6A-1/CRH6A-2, D_{appr}_CRH6A-2/CRH6A-1,D_{EBPS}_CRH6A-2/CRH6A-1, and D_{CBCS}_CRH6A-2/CRH6A-1, are used to identify the variation of train separation deviation and speed differential across the whole railway corridor, which are reported in Fig. 14, where solid profiles versus time show the real-time separation deviations between the actual separation and the service separation, and dashed profiles versus time represent real-time velocity differences between the follower and the leader. The speed profile versus time of the leader is also illustrated in Fig. 14 as a reference.

The aforementioned KPIs of the simulation results of all cases are summarized in Table 6, including the average train separation (s_{ave}); the maximum negative separation deviation ($d_{ne,max}$); total time the maximum change rate of control is reached (t_{ii_max}); the number of emergency separation infringements (n_{in}); the total duration of emergency separation infringements (t_{in}), the maximum infringement distance ($d_{in,max}$), and the maximum negative emergency separation error ($e_{ne,max}$).

First, according to Table 6, no collision occurred in any of the experimental cases. Furthermore, no infringements of emergency separation were observed in cases D_{CBCS}_CRH6A-1/CRH6A-2 and D_{CBCS}_CRH6A-2/CRH6A-1 (where the proposed methods were applied), and D_{EBPS}_CRH6A-2/CRH6A-1 where, however, the maximum negative emergency separation error ($e_{ne,max}$) was observed as −3.30 m. Introducing a constant impact distance, as commonly applied in the existing literature on the APF algorithm, does not improve train control performance, but instead, it leads to emergency separation infringements in these three cases. For instance, in case D_{CBCS}_CRH6A-1/CRH6A-2_c, an infringement of 13.2 s was observed compared to case D_{CBCS}_CRH6A-1/CRH6A-2.

According to Table 6, significant increases in the average train separation are observed in the cases exploiting the combination of CRH6A-2/CRH6A-1 compared with the combination of CRH6A-1/CRH6A-2. For instance, in Table 6, the average train separation is 67.94 m in Case D_{CBCS}_CRH6A-1/CRH6A-2, however, it reaches 478.05 m in Case D_{CBCS}_CRH6A-2/CRH6A-1. The combination of CRH6A-1/CRH6A-2 also results in significant increases in the speed differential between the follower and the leader, comparing the dashed profiles of the speed difference in Fig. 14(a) with the dashed profiles in Fig. 14(b). For instance, the speed differential in Case D_{CBCS}_CRH6A-1/CRH6A-2 ranges from −3 km/h to 10.7 km/h according to Fig. 14(a), while according to Fig. 14(b), the speed differential in Case D_{CBCS}_CRH6A-2/CRH6A-1 ranges from −14 km/h to 35 km/h.

The results clearly show that low train control performances (e.g. fluctuating separation deviations as shown by the blue curve in Fig. 14(a)) are obtained when referring to an approximated train separation calculation (D_{appr}), because the emergency separation is often infringed by the follower, hence leading to unsafe train movements. For instance, according to Table 6, t_{in} in cases D_{appr}_CRH6A-1/CRH6A-2 and D_{appr}_CRH6A-2/CRH6A-1 reaches 7.4 s and 21.80 s, respectively, which implies the total time that the follower reaches risky VC movement by infringing the emergency position during the whole journey within the experimental railway corridor (recall the aforementioned definition of t_{in} in this section). These results align with the findings in Fig. 10 regarding the comparison between the emergency separation in D_{appr} and the benchmark. It should be noted that in order to have complete simulation results in all cases, we do not let the follower take an emergency braking when the train infringes the emergency position during simulation. However, in practical train operations under VC, an emergency braking should be triggered once the train exceeds the emergency position. A significant increase in the maximum negative separation deviation ($d_{ne,max}$) is also observed when exploiting D_{appr}, according to Table 6 and Fig. 14(b). For instance, in cases D_{appr}_CRH6A-1/CRH6A-2 and D_{appr}_CRH6A-2/CRH6A-1, the maximum negative separation deviation reaches −13.06 m and −11.78 m, respectively, according to Table 6.

When instead the APF-based train control refers to an End Braking Point Supervision, infringements of emergency separation were also observed. For instance, in case D_{EBPS}_CRH6A-1/CRH6A-2, three infringements with a total duration of 22.2 s (the highest among all cases) were recorded. Moreover, in the combination CRH6A-1/CRH6A-2, the follower train is provided with very jerky control indications. For instance, according to Fig. 13(a), in Case D_{EBPS}_CRH6A-1/CRH6A-2 where the APF-based controller operates the train with D_{EBPS}, significant fluctuations in control occur due to the computed service separation getting aggressively close to the emergency separation profile. This finding aligns also with the observations in Fig. 10, where the emergency separation using the EBPS method consistently falls significantly below the benchmark. Also, according to Table 6, in Case D_{EBPS}_CRH6A-1/CRH6A-2, t_{ii_max}, the overall time the maximum change rate of control is reached (recall the aforementioned definition of t_{ii_max}), reaches 12.7 s, which can be practically unmanageable by a train driver or the Automatic Train Operation (ATO), besides resulting in uncomfortable travel conditions for passengers.

When the complete braking procedures of trains are instead supervised (i.e., Complete Braking Curve Supervision), for whatever train leader–follower combination (i.e. either CRH6A-1/CRH6A-2 or CRH6A-2/CRH6A-1), the follower is controlled stably relying on the sole service braking without any triggering of emergency braking actions. For instance, n_{in}, t_{in} and $d_{in,max}$ are all 0 in both cases D_{CBCS}_CRH6A-1/CRH6A-2 and D_{CBCS}_CRH6A-2/CRH6A-1, as illustrated in Table 6. Results also show that the APF-based train control has the best performance in reducing the maximum negative separation deviation. For instance, the maximum negative separation

Table 6
KPI of simulation results.

Case	Collision (Yes/No)	s_{ave}(m)	$d_{ne,max}$(m)	t_{ti_max}(s)	n_{in}	t_{in}(s)	$d_{in,max}$(m)	$e_{ne,max}$(m)
D_{appr}_CRH6A-1/CRH6A-2	No	77.80	−13.06	3.0	2	7.4	1.15	−1.04
D_{EBPS}_CRH6A-1/CRH6A-2	No	55.99	−5.46	12.7	3	22.2	9.69	−37.86
D_{EBPS}_CRH6A-1/CRH6A-2_c	No	59.00	−30.29	3.1	1	8.1	1.86	−41.73
D_{CBCS}_CRH6A-1/CRH6A-2	No	67.94	−4.29	0.3	0	0	0	0
D_{CBCS}_CRH6A-1/CRH6A-2_c	No	68.81	−9.52	0.8	1	13.2	2.66	−1.60
D_{appr}_CRH6A-2/CRH6A-1	No	542.00	−11.78	0.4	1	21.80	10.65	−48.26
D_{EBPS}_CRH6A-2/CRH6A-1	No	478.05	−7.85	0.4	0	0	0	−3.30
D_{EBPS}_CRH6A-2/CRH6A-1_c	No	486.22	−16.52	0.8	1	15.2	7.68	−5.20
D_{CBCS}_CRH6A-2/CRH6A-1	No	478.05	−7.85	0.4	0	0	0	0
D_{CBCS}_CRH6A-2/CRH6A-1_c	No	486.22	−16.52	0.8	1	15.2	7.68	−5.20

deviation is −4.29 m in D_{CBCS}_CRH6A-1/CRH6A-2, while it's −13.06 m and −5.46 m in cases D_{appr}_CRH6A-1/CRH6A-2 and D_{EBPS}_CRH6A-1/CRH6A-2, respectively, according to Table 6. Additionally, it should be noted that in Table 6, t_{ti_max} at 0.3 s or 0.4 s refers to a short duration during which the follower reaches the maximum change rate of control due to the follower being in the maximum traction phase for departure.

Also note that the similar simulation results are observed for Case D_{EBPS}_CRH6A-2/CRH6A-1 and Case D_{CBCS}_CRH6A-2/CRH6A-1 according to Table 6. This is due to that when the follower has a lower braking capability compared to the leader, the safe train separation requirements calculated using CBCS and EBPS methods may converge. As a result, the train control indications generated under these two safe train separation supervision methods are similar since the potential fields which are built using the safe train separation requirements are similar. This suggests that the EBPS method, while ensuring train safety, can also be applicable in train convoys where the leader has a lower braking capability than the leader.

5. Conclusions

This paper proposed an Artificial Potential Field (APF)-based train control method to address Complete Braking Curve Supervision (CBCS)-based train safe separation under VC with Dynamic Safety Margin (DSM) taking into account comprehensive realistic factors, such as train heterogeneities, communication delay, unexpected emergency braking, positioning and velocity measurement errors, and more realistic train resistances and dynamics by a representation of a homogeneous strip train model. Case studies on real-line operation environments have been analyzed to compare control performances of the APF-based train control algorithms for cases that supervise either an approximated braking distance with flat track and no risk factors (cases with D_{appr}), an end-point braking distance (cases with D_{EBPS}) or the complete train braking process (cases with D_{CBCS}). For each of those cases, the performances of the APF-based controller are evaluated for different combinations of heterogenous trains in a VC convoy with respect to several KPIs including average train separation, maximum negative separation deviation, overall time the maximum change rate of control is reached, number of infringements, overall infringement duration of emergency separation, maximum infringement distance, and maximum negative emergency separation error. The results show that different combinations of heterogeneous trains have significant impacts on the control performance under VC. The combination CRH6A-1/CRH6A-2 where the leader has a lower braking capability, shows significantly reduced train separations and speed differences compared to cases with the combination CRH6A-2/CRH6A-1 where the follower has a lower braking capability than the leader. Results also show that different train separations with DSM also have great impacts on control performance. CBCS-based train separation with DSM (D_{CBCS}) exhibits the best control performance in reducing train separation deviations and ensuring train safety by avoiding emergency separation infringements and train collisions under VC. In contrast, both the approximated and EBPS-based train separations with DSM (i.e. D_{appr} and D_{EBPS}) can lead to significant fluctuations in controller outputs (particularly when the case exploits the combination CRH6A-1/CRH6A-2), which should be avoided in practice. Furthermore, a crucial safety concern is that exploiting EBPS-based train separations (D_{appr} and D_{EBPS}) result in emergency separation infringements, which should also be avoided in practical train operations. Therefore, in this paper, the proposed APF-based VC train control algorithm for Complete Braking Curve Supervision with DSM shows alignment with safety and real-time performance requirements necessary to safely separate trains under VC signalling. The experimental results hence suggest the method as promising for a potential future piloting in real-life operations.

Since we assume the leader train respects the planned speed indications in this paper, further research will be devoted to including the leader's actual control strategy which may result in differences between the leader's actual and planned speed profiles. A comparison between the proposed and the existing APF approaches is also considered one of the interesting research directions in our follow-up research.

CRediT authorship contribution statement

Yuqing Ji: Writing – review & editing, Writing – original draft, Validation, Software, Methodology, Conceptualization. **Egidio Quaglietta:** Writing – review & editing, Supervision, Methodology, Conceptualization. **Rob M.P. Goverde:** Writing – review & editing, Supervision, Methodology. **Dongxiu Ou:** Validation, Supervision, Methodology, Conceptualization.

Declaration of competing interest

The authors declare that they have no known competing financial interests or personal relationships that could have appeared to influence the work reported in this paper.

Acknowledgement

This research was supported by the National Natural Science Foundation of China (52172329), China Scholarship Council (202206260136) and the Fundamental Research Funds for the Central Universities (2023-4-ZD-03).

References

Aoun, J., Quaglietta, E., Goverde, R.M.P., 2023. Roadmap development for the deployment of virtual coupling in railway signalling. *Technol. Forecast. Soc. Chang.* 189, 122263.

Arel, I., Liu, C., Urbanik, T., Kohls, A.G., 2010. Reinforcement learning-based multi-agent system for network traffic signal control. *IET Intel. Transport Syst.* 4, 128–135.

Basile, D., ter Beek, M.H., Ferrari, A., Legay, A., 2022. Exploring the ERTMS/ETCS full moving block specification: an experience with formal methods. *Int. J. Softw. Tools Technol. Transfer* 24, 351–370.

Bock, U., 1999. Erhoehung der Streckenauslastung durch“ Virtuelle Zugverbaende”. *VDI-Berichte*.

Buşoniu, L., Babuška, R., De Schutter, B., 2010. Multi-agent reinforcement learning: an overview. Innovations in multi-agent systems and applications-1, 183-221.

Cao, Y., Wen, J., Hobiny, A., Li, P., Wen, T., 2022. Parameter-varying artificial potential field control of virtual coupling system with nonlinear dynamics. *Fractals* 30, 2240099.

Cao, Y., Wen, J., Ma, L., 2021. Tracking and collision avoidance of virtual coupling train control system. *Futur. Gener. Comput. Syst.* 120, 76–90.

Chai, M., Wang, H., Tang, T., Chai, J., Liu, H., 2023. A relative operation-based separation model for safe distances of virtually coupled trains. *IEEE Trans. Intell. Veh.*

Chen, D., Cheng, R., Chen, D., Cheng, R., 2019. Incremental train control system of Qinghai–Tibet railway. Intell. Process. Algorith. Appl. GPS Position. Data of Qinghai-Tibet Railway 35–50.

Chen, M., Xun, J., Liu, Y., 2020. A coordinated collision mitigation approach for virtual coupling trains by using model predictive control. 2020 IEEE 23rd International Conference on Intelligent Transportation Systems (ITSC), 2020. IEEE, 1-6.

Chen, Y., Luo, G., Mei, Y., Yu, J., Su, X., 2016. UAV path planning using artificial potential field method updated by optimal control theory. *Int. J. Syst. Sci.* 47, 1407–1420.

Davis, W.J., 1926. The tractive resistance of electric locomotives and cars, General Electric.

de Rivera, A.D., Dick, C.T., 2021. Illustrating the implications of moving blocks on railway traffic flow behavior with fundamental diagrams. Transp. Res. Part C Emerging Technol. 123, 102982.

Di Meo, C., Di Vaio, M., Flammini, F., Nardone, R., Santini, S., Vittorini, V., 2019. ERTMS/ETCS virtual coupling: proof of concept and numerical analysis. *IEEE Trans. Intell. Transp. Syst.* 21, 2545–2556.

Dick, C.T., Mussanov, D., Evans, L.E., Roscoe, G.S., Chang, T.-Y., 2019. Relative capacity and performance of fixed-and moving-block control systems on North American freight railway lines and shared passenger corridors. *Transp. Res. Rec.* 2673, 250–261.

Diehl, M., Ferreau, H.J., Haverbeke, N., 2009. Efficient numerical methods for nonlinear MPC and moving horizon estimation. Nonlinear Model Predict. Control: Towards New Challenging Appl. 391–417.

Duhé, J.-F., Victor, S., Melchior, P., 2021. Contributions on artificial potential field method for effective obstacle avoidance. *Fract. Calc. Appl. Anal.* 24, 421–446.

Europe’s Rail, 2018. [Online]. Available: https://cordis.europa.eu/project/id/826347 [Accessed 27th February 2024].

Fan, B., 2012. Railway traffic rescheduling approaches to minimise delays in disturbed conditions. PhD, University of Birmingham.

Felez, J., Kim, Y., Borrelli, F., 2019. A model predictive control approach for virtual coupling in railways. IEEE Trans. Intell. Transp. Syst. 20, 2728–2739.

Ferreau, H.J., Bock, H.G., Diehl, M., 2008. An online active set strategy to overcome the limitations of explicit MPC. *Int. J. Robust Nonlinear Control: IFAC-affiliated J.* 18, 816–830.

Filipović, Ž., 2015. Elektrische Bahnen: Grundlagen, Triebfahrzeuge, Stromversorgung, Springer-Verlag.

Flammini, F., Marrone, S., Nardone, R., Petrillo, A., Santini, S., Vittorini, V., 2018. Towards railway virtual coupling. 2018 IEEE International Conference on Electrical Systems for Aircraft, Railway, Ship Propulsion and Road Vehicles & International Transportation Electrification Conference (ESARS-ITEC), 2018. IEEE, 1-6.

Guo, Z., Li, Z., 2023. Virtual coupling of permanent magnetic maglev trains: an improved cooperative tracking and collision avoidance control protocol. *IET Intel. Transport Syst.*

Han, Y., Zhang, K., Li, H., Coelho, E.A.A., Guerrero, J.M., 2017. MAS-based distributed coordinated control and optimization in microgrid and microgrid clusters: a comprehensive overview. *IEEE Trans. Power Electron.* 33, 6488–6508.

Hansen, H.S., Nawaz, M.U., Olsson, N., 2017. Using operational data to estimate the running resistance of trains. Estimation of the resistance in a set of Norwegian tunnels. *J. Rail Transp. Plann. Manage.* 7, 62–76.

Ketphat, N., Whiteing, A., Liu, R., 2022. State movement for controlling trains operating under the virtual coupling system. *Proc. Inst. Mech. Eng., Part F: J. Rail Rapid Transit* 236, 172–182.

Khatib, O., 1986. Real-time obstacle avoidance for manipulators and mobile robots. *Int. J. Robot. Res.* 5, 90–98.

Li, S.E., Zheng, Y., Li, K., Wang, L.-Y., Zhang, H., 2017. Platoon control of connected vehicles from a networked control perspective: literature review, component modeling, and controller synthesis. *IEEE Trans. Veh. Technol.*

Liu, Y., Ou, D., Yang, Y., Dong, D., 2023. A method for maintaining virtually coupled states of train convoys. *Proc. Inst. Mech. Eng., Part F: J. Rail Rapid Transit* 237, 243–252.

Lu, X., Lu, R., Chen, S., Lu, J., 2012. Finite-time distributed tracking control for multi-agent systems with a virtual leader. *IEEE Trans. Circuits Syst. I Regul. Pap.* 60, 352–362.

Luo, X., Tang, T., Yin, J., Liu, H., 2023. A robust mpc approach with controller tuning for close following operation of virtually coupled train set. *Transp. Res. Part C Emerging Technol.* 151, 104116.

Ma, F., He, Z., Xu, Q., Luo, A., Zhou, L., Li, M., 2016. Multilevel power conditioner and its model predictive control for railway traction system. *IEEE Trans. Ind. Electron.* 63, 7275–7285.

Ning, B., 1998. Absolute braking and relative distance braking-train operation control modes in moving block systems. *WIT Trans. Built Environ.*

Ning, Z., Ou, D., Xie, C., Zhang, L., Gao, B., He, J., 2023. Optimal convoy composition for virtual coupling trains at junctions: a coalition formation game approach. *Transp. Res. Part C Emerging Technol.* 154, 104277.

Park, J., Lee, B.-H., Eun, Y., 2020. Virtual coupling of railway vehicles: gap reference for merge and separation, robust control, and position measurement. *IEEE Trans. Intell. Transp. Syst.* 23, 1085–1096.

Park, M.G., Jeon, J.H., Lee, M.C., 2001. Obstacle avoidance for mobile robots using artificial potential field approach with simulated annealing. ISIE 2001. 2001 IEEE International Symposium on Industrial Electronics Proceedings (Cat. No. 01TH8570), 2001. IEEE, 1530-1535.

Porfiri, M., Roberson, D.G., Stilwell, D.J., 2007. Tracking and formation control of multiple autonomous agents: a two-level consensus approach. *Automatica* 43, 1318–1328.

Quaglietta, E., Spartalis, P., Wang, M., Goverde, R.M.P., van Koningsbruggen, P., 2022. Modelling and analysis of virtual coupling with dynamic safety margin considering risk factors in railway operations. *J. Rail Transp. Plann. Manage.* 22, 100313.
Quaglietta, E., Wang, M., Goverde, R.M.P., 2020. A multi-state train-following model for the analysis of virtual coupling railway operations. *J. Rail Transp. Plann. Manage.* 15, 100195.
Rahmani, A., Ji, M., Mesbahi, M., Egerstedt, M., 2009. Controllability of multi-agent systems from a graph-theoretic perspective. *SIAM J. Control Optim.* 48, 162–186.
Ren, W., 2008. Decentralization of virtual structures in formation control of multiple vehicle systems via consensus strategies. *Eur. J. Control.* 14, 93–103.
Rostami, S.M.H., Sangaiah, A.K., Wang, J., Liu, X., 2019. Obstacle avoidance of mobile robots using modified artificial potential field algorithm. *EURASIP J. Wirel. Commun. Netw.* 2019, 1–19.
Rubagotti, M., Raimondo, D.M., Ferrara, A., Magni, L., 2010. Robust model predictive control with integral sliding mode in continuous-time sampled-data nonlinear systems. *IEEE Trans. Autom. Control* 56, 556–570.
Sharma, S.K., Kumar, A., 2018. Impact of longitudinal train dynamics on train operations: a simulation-based study. *J. Vib. Eng. Technol.* 6, 197–203.
Shift2Rail 2018. [Online]. Available: https://projects.shift2rail.org/s2r_ip_TD_D.aspx?ip=2&td=aa1f0995-1402-4e7b-a905-49fba1bc6f71 [Accessed 27th February 2024].
Su, S., Liu, W., Zhu, Q., Li, R., Tang, T., Lv, J., 2022. A cooperative collision-avoidance control methodology for virtual coupling trains. *Accid. Anal. Prev.* 173, 106703.
Su, S., She, J., Wang, D., Gong, S., Zhou, Y., 2023. A stabilized virtual coupling scheme for a train set with heterogeneous braking dynamics capability. *Transp. Res. Part C Emerging Technol.* 146, 103947.
Sun, J., Tang, J., Lao, S., 2017. Collision avoidance for cooperative UAVs with optimized artificial potential field algorithm. *IEEE Access* 5, 18382–18390.
Tian, Z., Zhao, N., Hillmansen, S., Roberts, C., Dowens, T., Kerr, C., 2019. SmartDrive: traction energy optimization and applications in rail systems. *IEEE Trans. Intell. Transp. Syst.* 20, 2764–2773.
Versluis, N.D., Quaglietta, E., Goverde, R.M.P., Pellegrini, P., Rodriguez, J., 2024. Real-time railway traffic management under moving-block signalling: a literature review and research agenda. *Transp. Res. Part C Emerging Technol.* 158, 104438.
Wang, H., Zhao, Q., Lin, S., Cui, D., Luo, C., Zhu, L., Wang, X., Tang, T., 2020. A reinforcement learning empowered cooperative control approach for IIoT-based virtually coupled train sets. *IEEE Trans. Ind. Inf.* 17, 4935–4945.
Wang, J., Liu, H., Tang, T., Luo, X. & Chai, M. A space-time interval based protection method for virtual coupling. 2022 China Automation Congress (CAC), 2022. IEEE, 4906-4911.
Wang, P., Gao, S., Li, L., Sun, B., Cheng, S., 2019. Obstacle avoidance path planning design for autonomous driving vehicles based on an improved artificial potential field algorithm. *Energies* 12, 2342.
Wolf, M.T., Burdick, J.W., 2008. Artificial potential functions for highway driving with collision avoidance. 2008 IEEE International Conference on Robotics and Automation, 2008. IEEE, 3731-3736.
Wu, Q., Ge, X., Han, Q., Wang, B., Wu, H., Cole, C., Spiryagin, M., 2023. Dynamics and control simulation of railway virtual coupling. *Veh. Syst. Dyn.* 61, 2292–2316.
Xue, D., Yao, J., Chen, G., Yu, Y.-L., 2010. Formation control of networked multi-agent systems. *IET Control Theory Appl.* 4, 2168–2176.
Xun, J., Chen, M., Liu, Y., Liu, F., 2020. An overspeed protection mechanism for virtual coupling in railway. *IEEE Access* 8, 187400–187410.
Zhang, Q., Wang, H., Zhang, Y., Chai, M., 2023. An adaptive safety control approach for virtual coupling system with model parametric uncertainties. *Transp. Res. Part C Emerging Technol.* 154, 104235.
Zheng, Y., Zhu, Y., Wang, L., 2011. Consensus of heterogeneous multi-agent systems. *IET Control Theory Appl.* 5, 1881–1888.